2005

Characteristics of confined square jets in the vicinity of a free surface.

Girish Sankar
University of Windsor

CHARACTERISTICS OF CONFINED SQUARE JETS IN THE VICINITY OF A FREE SURFACE

by

Girish Sankar

A Thesis

Submitted to the Faculty of Graduate Studies and Research

through the Department of Civil and Environmental Engineering

in Partial Fulfillment of the Requirements for

the Degree of Master of Applied Science at the

University of Windsor

Windsor, Ontario, Canada

2005

Your file Votre référence
ISBN: 0-494-09645-4
Our file Notre référence
ISBN: 0-494-09645-4

ABSTRACT

The results of an experimental investigation of a turbulent jet flow issuing from a square nozzle in the vicinity of a free surface are presented. Experiments were conducted using a two-dimensional laser Doppler anemometer and a particle image velocimeter. The focus of this study was the near region of the jet (X/B < 30). Here, B refers to the nozzle width and X is the distance from the nozzle exit. LDA measurements were conducted at eight stations downstream of the nozzle exit along the centreline of the jet. Four tailwater depths were used in this study. Additional measurements were also conducted to identify axis switching and to this end measurements were obtained at various transverse locations. PIV measurements were conducted in the near-jet region (X/B < 3) corresponding to a tailwater depth of 2.5B.

A good comprehension of the fluid dynamics of a square jet expanding in the vicinity of the free surface is achieved. Square jets in the vicinity of the free surface behave quite differently from conventional axisymmetric jets. The traditional growth and evolution of flow conditions such as extent of zone of flow establishment and zone of established flow are not noticed in this study. The jet completely loses its form by 27 nozzle widths after interacting with the free surface.

Higher order moments were calculated to provide information on the coherent structures and study the role of velocity fluctuations. Two local peaks on either side of the jet centerline is observed. The difference in magnitudes of the peaks indicate differences in the prevailing entrainment characteristics on the top and bottom portions of the jet. Through the quadrant analysis, sweep and ejection type events were observed.

To better understand these events, four kinds of eddies are classified for simplicity and their behavior is discussed.

LDA and PIV comparison show good agreement in describing the flow configuration and the mean velocity field at different downstream locations. The PIV measurements aid in qualitatively deciphering vortical structures. A Galilean transformation was carried out to distinguish vortex structures.

ACKNOWLEDGEMENT

The long journey of my Masters program is coming to an end with the help of the following people.

Thanks to my parents who have supported me throughout.

My sincere gratitude and profound appreciation to my supervisors, Dr. Ram Balachandar and Dr. Rupp Carriveau for their patience, invaluable supervision, guidance, thoughtful insights.

Gratitude is also expressed to Dr. Ron Barron, Dr. David Ting and Dr. Rajesh Seth the members of the examination committee, for their helpful comments, suggestions and encouragement.

My thanks to Mr. Richard Clark and Mr. Lucien Pop for their prompt help and support in building and maintaining the experimental setup.

TABLE OF CONTENTS

LIST OF TABLES

LIST OF FIGURES

NOMENCLATURE

ACRONYMS

2-D = Two-dimensional

LDA = Laser Doppler Anemometer

PIV = Particle Image Velocimetry

r.m.s = root mean square

TW = Tail water

ENGLISH SYMBOLS

B = width of the nozzle

g = gravitational acceleration

$D_u = \overline{u^2 v}$

$D_v = \overline{v^2 u}$

H = tailwater depth

u = instantaneous mean velocity in the streamwise direction

$\overline{uv}$ = turbulent shear stress

$\overline{u^2 v}$ = turbulent diffusion in the normal direction

u'^2 = streamwise turbulence intensity

$\overline{u^3}$ = streamwise flux of streamwise momentum $\overline{u^2}$

$\overline{U}$ = mean velocity at any point in streamwise direction

U_j = jet exit velocity

U_{cl}, U_o = Centerline velocity at any station along x-direction

v'^2 = normal turbulence intensity

$\overline{v^2}u$ =turbulent diffusion in the streamwise direction

$\overline{v^3}$ = normal flux of v momentum

X = longitudinal distance from the nozzle

Y = lateral distance from the nozzle

$y_{1/2}$ = value of y where velocity is $U_m/2$

Z = lateral distance from the centreline

GREEK SYMBOLS

ν = kinematic viscosity

ρ = mass density of water

δ = Velocity Half- width

CHAPTER 1

INTRODUCTION

Turbulent jets find applications in diverse fields of engineering. Due to the varied applications, the characteristics of turbulent jets are perhaps one of the most studied problems in fluid mechanics. It is important to understand the dynamics of mixing and propose some means of control and improve mixing. In this context there is crucial interest in identifying and understanding the local nature of the jet and their evolution in space and time.

A review of literature indicates that the characteristics of jets can be influenced by the design of nozzle geometry (nozzle shape, nozzle cross- section) and the ambient conditions surrounding the jet. A jet is commonly classified as a free jet (unconfined) when it is not influenced by any physical/fluid structures surrounding the jet. The jet is also commonly defined as axisymmetric when it emanates from a circular cross-sectional area. Extensive measurements in the self similar region of the axisymmetric jet have been reported by Wygnanski and Fielder (1969). Previous analyses have shown the existence of a self preserving state. However this state is uniquely defined by the conditions prevailing at the nozzle exit. In this regard attention has recently moved to the near exit flow field to account for the effects of mixing due to large scale vortical structures.

Non-circular jets can have enhanced entrainment properties relative to comparable circular jets, due to axis rotation of the jet cross section resulting from deformation of vortex rings with non-uniform curvature. Due to their enhanced mixing properties non-circular jets find their applications in devices where mixing is a subject of vital importance.

The first systematic investigation of three-dimensional jet was performed by Sforza, Steiger and Trentacose (1965).

It should be remarked that the characteristics of jets in confined situations have been studied to a lesser extent even though a number of practical situations reflect a confined three-dimensional analysis. Several researchers have studied the characteristics of jets considering them to be free jets neglecting the fact that they were partly or fully confined. This observation was noted in a study by Hussein et al., (1994). The confinement can occur either in the form of a solid wall or a free surface.

Jet dynamics below a free surface plays an important role in diverse areas ranging from environmental flows such as discharge of pollutant in a shallow river and industrial mixing processes. The behavior of turbulent flows adjacent to a free surface is of considerable interest to the remote detection of wakes of surface ships. Bernal and Madina (1988) investigated a round turbulent jet interacting with the free surface. Liepmann (1990) showed that free surface can strongly influence the instabilities in the near-field region of a round jet. The existence of orderly structure in the near-exit field has been recognized for some time. The large-scale structures control the initial growth of turbulent jets. They are generated in the shear layer produced in the jet exit.

Literature provides very less information about the characteristics of a jet emanating from a square cross-section that interacts with the free surface. To this end, an experimental study of the characteristics of a jet confined by solid walls on three sides and a free surface on the other has been carried out. This project is a part of larger study being carried out at the University of Windsor to understand the behavior of three-dimensional jets.

1.1 Objectives of the study

The objectives of this study are:

1) To understand the behavior and mixing processes in confined square jets in the vicinity of the free surface.

2) To study the tailwater effect on the jet development.

3) To investigate turbulent structures in the near jet region.

1.2 Organization of the thesis

This thesis is organized in the following manner. Literature review on jet characteristics is presented in Chapter 2. The experimental set-up and the procedures adopted are illustrated in Chapter 3. The results obtained are discussed in Chapter 4. Chapter 5 presents the recommendations for further studies.

CHAPTER 2

LITERATURE REVIEW

2.1 General Classification of jets

Jets are commonly classified as two-dimensional or three-dimensional depending upon the number of degrees of freedom. Further, jets can be either free or confined depending on the boundary conditions. Table 1 shows the common types of jets. Two-dimensional turbulent jets are further divided into two main types:

1) Plane turbulent free jets
2) Circular Jets

Both these types of jets have several common characteristics. Generally there are two distinct regions that are identified, ZFE (zone of flow establishment) and ZEF (zone of established flow). In the ZEF region, the jet tends to be in a self-preserving state with a typical Gaussian type velocity distribution. For clarity, circular free jets are discussed in some detail.

2.2 Circular free jets:

The axisymmetric or round jet has been the subject of many studies over the years as it is considered as a benchmark for research into the understanding of turbulent flows. There has been considerable work done devoted to the characteristics of axisymmetric free jets. Abramovich (1963) and Rajaratnam (1976) offer comprehensive reviews. Detailed description and analyses are presented by Wygnanski and Fielder (1969), Capp (1983), Xu and Antonia (2002), Rahman et al., (1997), Cenedese et al., (1994) and Warda et al., (1998).

Free Jet	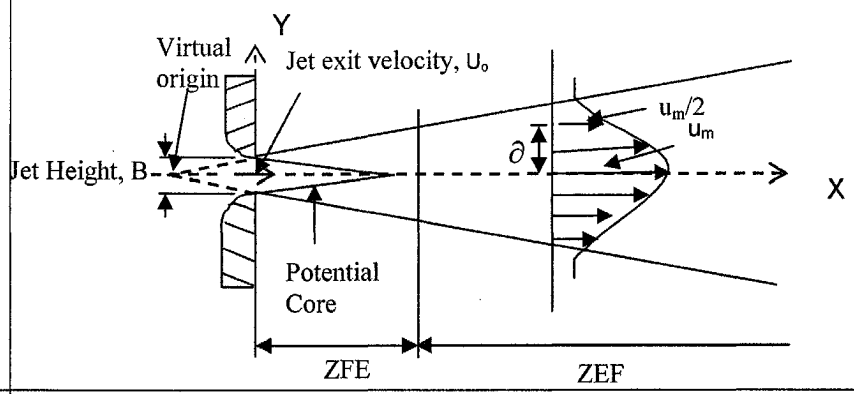
Wall Jet	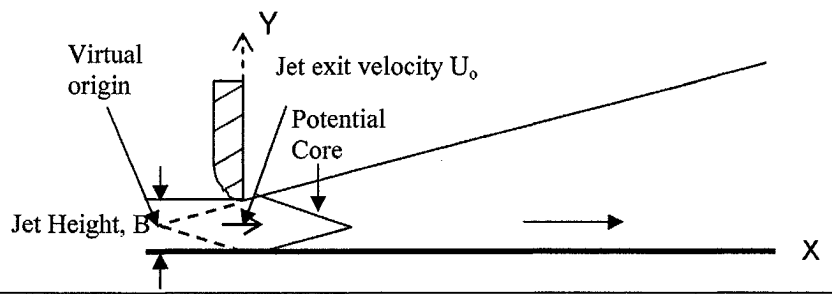
Impinging Jet	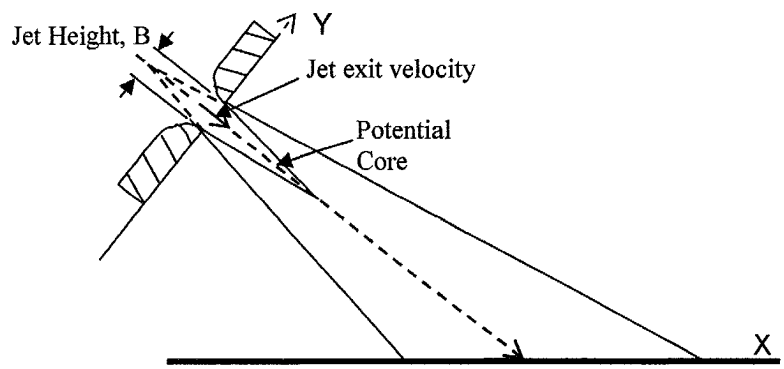
Offset Jet	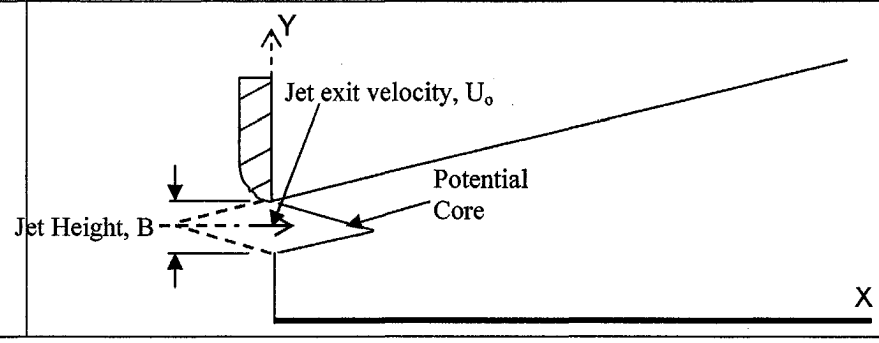

Table 1: Types of jets

Wygnanski and Fielder (1969) investigated an axisymmetric turbulent incompressible jet using linearized constant-temperature hot-wire anemometers. Most of the measurements were made at stations of 70 diameters downstream of the nozzle at high Reynolds number $\approx 10^5$. They found that the longitudinal fluctuations become self-similar at 40 diameters downstream, whereas the radial and tangential turbulence intensities attained similarity some 70 diameters from the nozzle where they reached a self preserving state. Later studies have shown that the distance required to attain self-preservation depends on the initial momentum thickness and turbulence intensity (Hussain and Zedan, 1978a, b). The spread rate and peak turbulent intensity in the self-preserving region depends on the initial boundary layer being laminar or turbulent. Hussein et al., (1994) performed experiments on a round free jet with hot-wire anemometer. They proposed an equation for the centerline velocity of a self-preserving jet as $U_C = \frac{BM_O^{1/2}}{(x - x_0)}$ where U_c is the centerline velocity, x_0 represents the virtual origin. Also, for a jet emanating from a nozzle with a top-hat velocity profile, they proposed that:

$$\frac{U_0}{U_c} = \frac{1}{B_u}\left(\frac{x}{D} - \frac{x_0}{D}\right)$$

Here, $B_u = \frac{1}{2}\pi^{\frac{1}{2}} B$, B is a constant.

Hussein et al., (1994) found that when normalized by proper length and velocity scales, the mean velocity profiles, turbulence intensities and shear stress at various axial stations collapsed onto single profiles. They noted that for the far field data X/D >50 of Wygnanski and Fielder (1969), the centerline mean velocity decay constant failed to stabilize to a constant value. The same discrepancy was observed in the LDA data of Capp

(1983). They concluded that the differences in these results were attributed to the smaller enclosures leading to confinement effects.

It can be seen that earlier investigators were keen on studying the far jet region. Attention has recently moved to the near jet region to account for the mixing due to large scale vortical structures. When round jets are influenced by one or more boundaries or due to the free surface the mixing processes get complicated and they start behaving like a three - dimensional jet. These jets are called as confined jets. Confinement is discussed in detail later.

2.4 Non Circular jets:

The flow fields of non- circular jets are characterized by 3 distinct regions. They are,

1) Potential core region: In this region the mixing initiated at the jet boundaries has not yet permeated the entire flow field, and is defined by a constant axial velocity close to the jet exit velocity. This region has characteristics similar to that of a circular jet. Further, the turbulence levels are close to zero.

2) Characteristic decay region: In this region the axial velocity decay is dependent upon orifice configuration, and velocity profiles in the plane of the minor axis are found to be similar, whereas those in the plane of major axis are non-similar. Hence, this region is termed "characteristic" of the initial geometry and is quite distinct from that noted in a circular jet.

3) Axisymmetric type decay: The axial velocity decay in this region is axisymmetric in nature, and the entire flow is found to approach axisymmetric conditions. Profiles in both symmetry planes in this region are found to be similar.

Miller et al., (1995) performed a simulation of spatially developing three-dimensional jets issued from circular and non - circular jets. He found that non - circular jets are more efficient mixers than circular jets. In a computational and experimental investigation by Grinstein et al., (1999), they found that the non - circular jets have enhanced entrainment properties relative to circular jets.

2.4.1 Square Jets:

Square jets being the subject of the present investigation is discussed in some detail below. Square jets are efficient mixers. This is due to the evolution of vortical structures that are formed as a result of instabilities in the initial region in these jets. Unlike a round vortical structure that has constant curvature, square jets have azimuthal curvature variation as a result of which the vortex ring deforms. This makes square jet an interesting topic to study.

Sforza, Steiger and Trentacose (1965)

Experiments were conducted in the far field region (30 diameters or more) to study rectangular, square and round jets. Sforza et al., (1965) noticed that the axial velocity distributions of non-circular jets are slightly different to those of axisymmetric jets. The difference from the similarity was due to secondary motion that may be initiated at the sharp corners and the shifts in the potential core region (due to the difference in the half - widths).

Duplessis, Wang and Kahawita (1974)

Duplessis et al., investigated the near field region of a half-inch square jet (first 20 diameters) at two exit velocities, where the jet behavior depends on the orifice geometry

and its initial velocity profiles. The jet with the lower velocity decays faster with a slower spreading rate while the jet with the higher velocity decays slowly with a higher spreading rate.

Quinn and Militzer (1988)

Quinn and Militzer (1988) performed experiments on a square jet. It was found that the square jet spreads faster than the axisymmetric jet having the same exit area. They also reported the existence of mean streamwise velocity off-center peaks at $X/D_e = 0.28$. They also suggested an equation for the jet in the far field $\frac{b_{1/2}}{D_e} = K_s\left(\frac{X}{D_e} + C_g\right)$ where $b_{1/2}$ is the velocity average half-width of the jet, K_s is the spreading rate, and C_g is the geometric virtual origin of the jet. The spreading of the square jet in the far field is the same as that of the axisymmetric jet.

Quinn (1992)

Quinn conducted an experimental investigation to study the streamwise evolution of a square jet. The quantities measured using hot-wire anemometry included the three components of the mean velocity vector, three Reynolds normal stresses, and two Reynolds primary shear stresses. He found that the near region of the jet is dominated by four sets of counter-rotating streamwise vortices. Quinn (1992) concluded that the off-center mean velocity peaks at $X/D_e = 0.28$ noted in the investigation by Quinn and Militzer (1988) was due to the existence of vena contracta, that is triggered by sharp edged exit of the square slot. Mean streamwise velocity contour maps were plotted and at about $X/D_e =$ 0.25 the contours had acquired a diamond shape and this shape was present up to $X/D_e =$

5.0, and the spacing between the contours increased indicating more significant entrainment of ambient fluid.

2.5 Confined Jets:

In many engineering applications, jets tend to be under confined conditions. Examples of such jets include cooling water discharge into river, lake or a pumped inflow of new water into a reservoir. The jet characteristics depend on the extent of confinement, proximity to the side walls (Figure 2.1) or vicinity to the free surface (Figure 2.2). Few studies have been carried out on confined jets even though a number of practical situations reflect a confined three-dimensional analysis. The following section is a review of literature on confined jets.

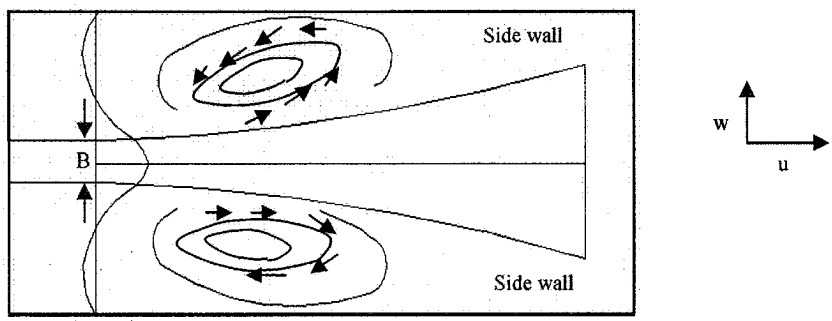

Figure 2.1. Schematic of side wall confinement

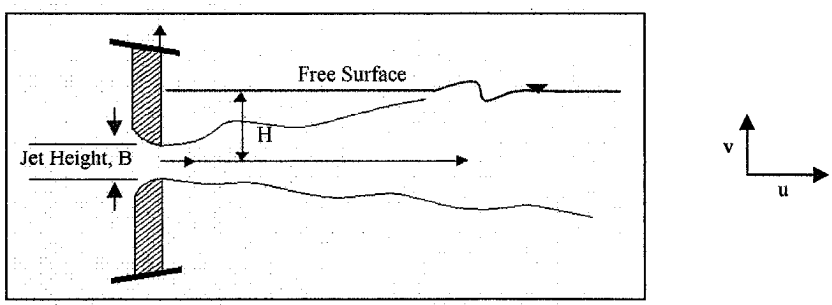

Figure 2.2. Schematic of free surface confinement

2.5.1 Confinement due to wall:

Foss and Jones (1968)

Foss and Jones investigated a bounded jet issuing from a rectangular orifice. It was found that the bounded jet had secondary flow structures developed at some distance from the orifice and these were attributed to vortex interaction between the free shear layers and the wall shear layers, thus showing the three-dimensional effects which make the flow even in the mid-plane between the bounding plates different from a two-dimensional jet.

Shineeb, Bugg and Balachandar (2002)

Shineeb et al., (2002) investigated an axisymmetric turbulent vertical jet yielding a Reynolds number of 21,900 with PIV. The jet was laterally and axially confined. The measurements show details of the velocity field in three regions of flow; the jet exit, near the centerline of the jet and near the top of the tank. They found that the axial confinement significantly influenced the centerline velocity at a distance of 13 nozzle diameters from the free surface.

2.5.2 Confinement due to free surface:

Rajaratnam and Humphires (1984)

They investigated the characteristics of plane and circular non-buoyant surface jet. They found that the velocity scales for the plane surface jet is about 0.9 times that for the plane jet and the velocity profiles are similar at different sections. For a circular surface jet they confirm the same scaling variables as that of the free jet. Also, the growth rate in the direction perpendicular to the free surface was found to be the same as the wall jet growth

rate, while the growth rate in the direction parallel to the surface is reduced by a factor of two compared to the wall case.

Bernal and Madina (1988)

Bernal and Madina investigated the interaction of a turbulent round jet with the free surface. Flow visualization of the free surface using a shadowgraph technique showed that surface waves were generated by the interaction of the jet with the free surface at sufficiently high speeds. They observed different dynamics at free surface (zero stress), compared to the solid wall (zero velocity), has an important effect in turbulent flow.

Anthony and Willmarth (1992)

Anthony and Willmarth studied the turbulence measurement in a round jet beneath a free surface using LDA. The measurements revealed that near the jet centerline, the rms fluctuations become anisotropic as the free surface was approached. They showed that the fluctuations normal to the surface were diminished, while those parallel to the surface were enhanced.

Liepman and Gharib (1994)

Liepman and Gharib investigated the vorticity and entrainment dynamics of near surface jets using PIV. They noticed that as the near surface jets develop, the maximum local vorticity initially behaved similar to a free surface jet, and then started to decay at a downstream location that was dependent on the Reynolds number. As the jet evolved downstream, the growth rate decreased. This was due to the hindering effect the surface had on entrainment.

2.5.3 Confinement due to wall and free surface:

Shineeb, Bugg and Balachandar (2004)

They investigated a round horizontal shallow jet, confined by the walls and by the free surface. The jet entrainment became complicated due to of the finite extent of ambient fluid above and below the jet. They showed variations in jet development from that of a free jet. They were one of the first to study the coherent structures in confined jets. They noticed the formation of clockwise and counter - clockwise vortices above and below the jet centerline. The counter - clockwise rotating structures appear below the centerline more often than clockwise rotating structures. These vortices changed in size as they progressed downstream. The existence of vortical structure in the near-jet region is a recent topic of study. There is evidence that these structures in the initial region are generated from the shear layer at the jet exit.

2.6 Evaluation of literature

The literature review has discussed the experimental and numerical studies contributing to our understanding of jets. The review reveals that there is renewed interest in the near-field area of the jet. Several researchers have neglected confinement effects and have considered confined jets to be free jets. This has led to discrepancies in understanding jets. Some of the other major influencing factors include the inlet geometry, the length-to-diameter ratio of the nozzle, the nature of the exit velocity profile and the associated boundary layer, exit turbulence intensity, exit Reynolds number and the conditions of the surrounding environment. The review also shows that there exists a difference in the self – preserving states attained by a particular type of flow having similar initial conditions.

An evaluation of the literature indicated that there is a need to understand the flow dynamics of three-dimensional jets. A comprehensive understanding of the temporal and spatial evolution of the complex fluid dynamic field in a turbulent square jet is yet to be obtained. The review also indicates that complete sets of turbulence quantities, e.g., the Reynolds stresses, triple correlations are scarce. The majority of coherent structure studies to date have been based on visualization and not on quantitative data. Studying the near region in jets by tracking the vortical structures will clearly aid in further understanding the jet dynamics. The present study will explore a practical scenario of a three-dimensional turbulent jet emanating from a square cross- section, and interacting with a free surface.

CHAPTER 3

EXPERIMENTAL SET-UP

3.1 The open channel flume

A schematic of the open channel flume and experimental setup used is shown in Figure 3.1. The rectangular flume was 9.5 m long, 1.2 m wide and 0.6 m. The side walls and bottom of the flume are made of Plexiglas to facilitate unobstructed transmission of laser beam and laser sheet into the flow. The tailgate controls the depth of the downstream water level.

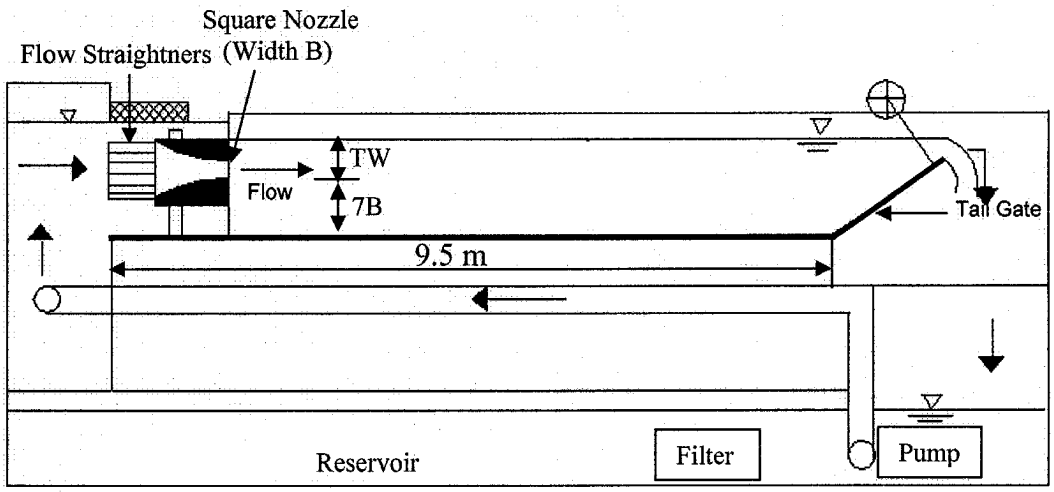

Figure 3.1 Schematic of the experimental setup

The supply system consisted of a pump, a head tank, and a flow control valve. The head tank was adjusted to deliver a constant velocity of 1 m/s at the nozzle exit. The tailwater (TW) depth measured from the bottom of the nozzle was varied from 1.5B to 5B.

3.2 Nozzle Design

A well-designed nozzle (Figure 3.2) with a square cross section (b = 40 mm) having a contraction ratio of 17: 1 was designed using a third degree polynomial (Morel, 1975). A

smooth contraction was adopted. It has been shown in earlier studies that the effluent jet tends to approach self-preservation rapidly with the use of a smooth contraction. It is important to recognize that a poorly designed exit condition can influence the growth of the jet (Romano, 2002). The nozzle axis was positioned at 0.3 m from the base of the flume with the aluminum angles. This effectively provided a jet, which could be potentially confined by solid walls on three sides and a free surface on the other.

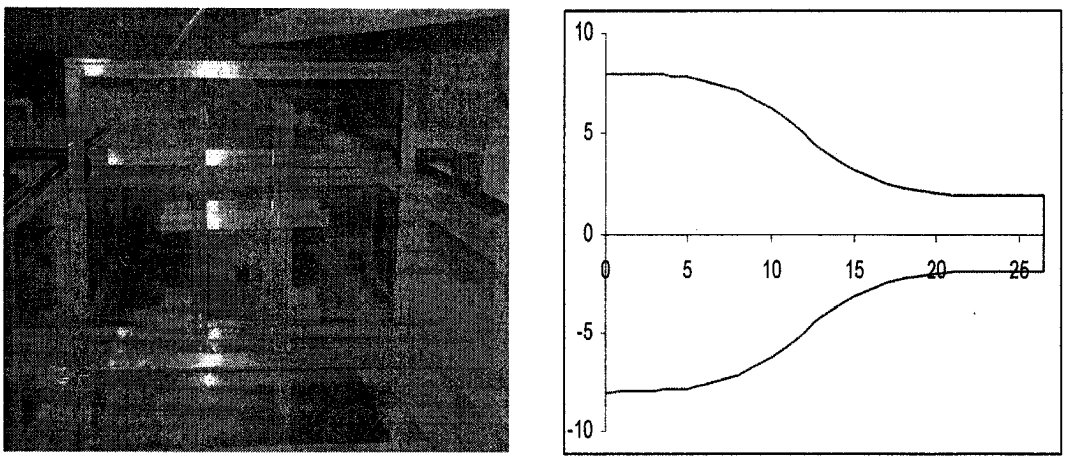

Figure 3.2 Nozzle and Nozzle contour details

3.3 Measurement Techniques

Measurements were conducted using a two dimensional Laser Doppler Velocimeter (LDV) system and a planar Particle Image Velocimeter (PIV) system. Data was obtained both in the jet developing region and at distances farther away from the nozzle exit. The distance from the nozzle axis to the free surface was varied by changing the tailwater level. Data was analyzed by choosing proper scaling variables that effectively described the flow field.

3.3.1 Laser Doppler Anemometry

Laser Doppler anemometry refers to the measurement of fluid velocity through the detection of the Doppler frequency shift of laser light that is shifted by small particles moving with the fluid. A typical system consists of a laser source, an optical arrangement, a photo-detector that converts light into electrical signals and signal processor.

The present LDA system was powered by 300 mW argon - ion laser. The optical system includes a Bragg cell. The laser beams of the same wavelength consisted of a shifted and an unshifted beam which intersected to form a control volume where the velocity was measured. The laser beam 514 nm was used to measure the streamwise component of velocity and the laser beam 488 nm measured the normal component of velocity. The measuring volume for the present configuration was $3.54\times10^{-10}\,m^3$. Due to the restriction imposed by the geometry of the transmitting optics, no measurements were possible at locations closer to 0.5B downstream of the nozzle exit. Measurements were conducted along the centerline of the jet at various distances downstream as summarized in Table 3. The measurement probe was mounted on a two-dimensional traversing system capable of traversing to the same location with an accuracy of ± 0.01mm. The traversing system was controlled by the computer. The flume water was filtered for several days prior to the start of the test and 5 micron diameter particles were added to the flow. The statistical parameters such as mean, root mean square and various other correlations were obtained using a Matlab® program.

3.3.2 Particle Image Velocimetry

Particle image velocimetry is a technique that employs tracer particles suspended in the flow to provide a two-dimensional map of the instantaneous velocity field. The centerplane section of the flow is illuminated by a light source and a sequence of images captured with a CCD camera is recorded with a specific time interval between images. The resulting picture is a sequence of images from the reflection of seeded particles as they travel in the illuminated flow plane. If the timing sequence of the illumination and the recording processes are synchronized correctly, the individual particles can be tracked between images. Velocities can be computed with the knowledge of time separation between images, correlations and displacements.

The present PIV system comprised of three sub-systems: the illumination system, consisting of Nd:YAG laser 532nm; imaging system, consisting of a CCD camera, timing system consisting of a synchronizer, and a computer equipped with frame - grabber hardware. This PIV system was configured to take sequential digital images of the seeded flow in groups of 500 image pairs at a sampling rate of 1 Hz. The mean velocity is calculated at each point in the measurement plane by taking the average of 2000 frame pairs.

3.4 Test Conditions

A summary of test conditions is presented in Table 3.1. Four different tailwater depths corresponding to 1.5B, 2.5B, 3.5B, 5B were chosen for this study. The height of the tailwater was measured from the bottom of the nozzle. The depth of water below the

nozzle was maintained at 7B for all the tailwater depths studied. The jet exit velocity was maintained at 1 m/s corresponding to a Reynolds number of (Rej = $U_j B/v$) 40,000.

3.5 Measurement Regions

Measurements were made in the flow field pertaining to the specific objectives listed previously in section 2.6. The following table shows how the measurement locations were chosen to meet the specific objectives.

Table 2. Measurement locations

Specific objectives	Measuring locations
1) Free Surface effects	1-D measurements made 10 mm below the free surface for all 4 tailwater depths
2) Velocity decay	2-D measurements along the centerline every 40 mm apart starting from X = 0.5B to 30B.
3) Axis Switching	2-D spanwise velocity profiles at lateral stations for a tailwater depth of 2.5B.
4)Jet behavior and turbulent structures	2-D spanwise velocity measurements were made at increasing downstream stations downstream namely X/B = 0.5, 1, 2, 3, 5, 10, 15, 27.

CHAPTER 4

RESULTS AND DISCUSSION

A qualitative description of the flow field is first provided. Dye injection aided in this observation. As the higher velocity flow exits the square nozzle into the ambient fluid, the jet retains its square cross - sectional shape upto a certain distance followed by an expansion in all directions. The jet first interacts with the free surface and after traveling further, it interacts with the bottom wall. For a tailwater depth of 2.5B, the impingement of the jet on the free surface occurs at about X = 5B from the nozzle, while impingement at the bottom wall occurs at about X = 20B. As one would expect, for the shallow tailwater depths, the impingement on the free surface occurs earlier. The ratio of the channel width to nozzle width is 30B and has relatively lower lateral confinement.

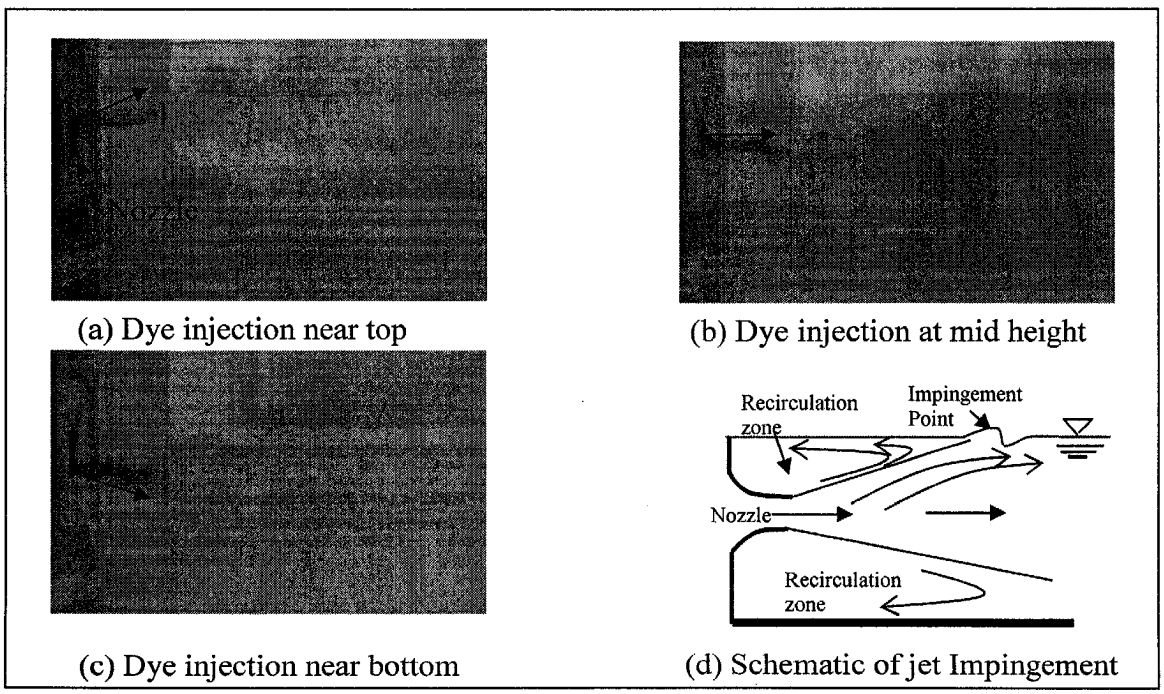

(a) Dye injection near top

(b) Dye injection at mid height

(c) Dye injection near bottom

(d) Schematic of jet Impingement

Figure 4.1 (a-d): Jet behavior at nozzle exit

The following pictures (4.1a – 4.1 c) show the behavior of the jet when the dye is introduced at different vertical locations at the nozzle exit. Figure 4.1(a) shows that the jet expands and impinges on the free surface around X = 5B. The free surface is obviously pliable and fluid impingement on it deforms the surface and waves are generated. The entrainment of ambient fluid into the jet, the deformation of the free surface and the formation of waves, cause the impingement point to move back and forth. One would be tempted to characterize an impingement region rather than a point. Figure 4.1(b) illustrates the existence of the undisturbed core region and Figure 4.1(c) shows the bottom expansion. Figure 4.1(d) illustrates an overall schematic view of the recirculating zone and the jet impingement on the free surface. It should be noted that in the recirculating zones, the flow is directed opposite to the main flow.

4.1 Mean Characteristics

For purposes of clarity, the mean velocity characteristics for the test with a tailwater depth of 2.5B is the first described. Following this, the turbulence intensity and higher order moments are discussed. Comparisons at other tailwater depths are also provided. The measurements reported, have their origin of the coordinate system on the jet centerline at the jet exit. The streamwise coordinate is x, positive downstream and the vertical coordinate is y, positive towards the free surface. The tests with a tailwater depth of 2.5 B was repeated several times to confirm the results

Figure 4.2 is a comprehensive description of the streamwise mean velocity field in the vertical central plane of the nozzle from the station nearest to the nozzle and extending to the last axial station (X/B = 27). The corresponding locations are identified

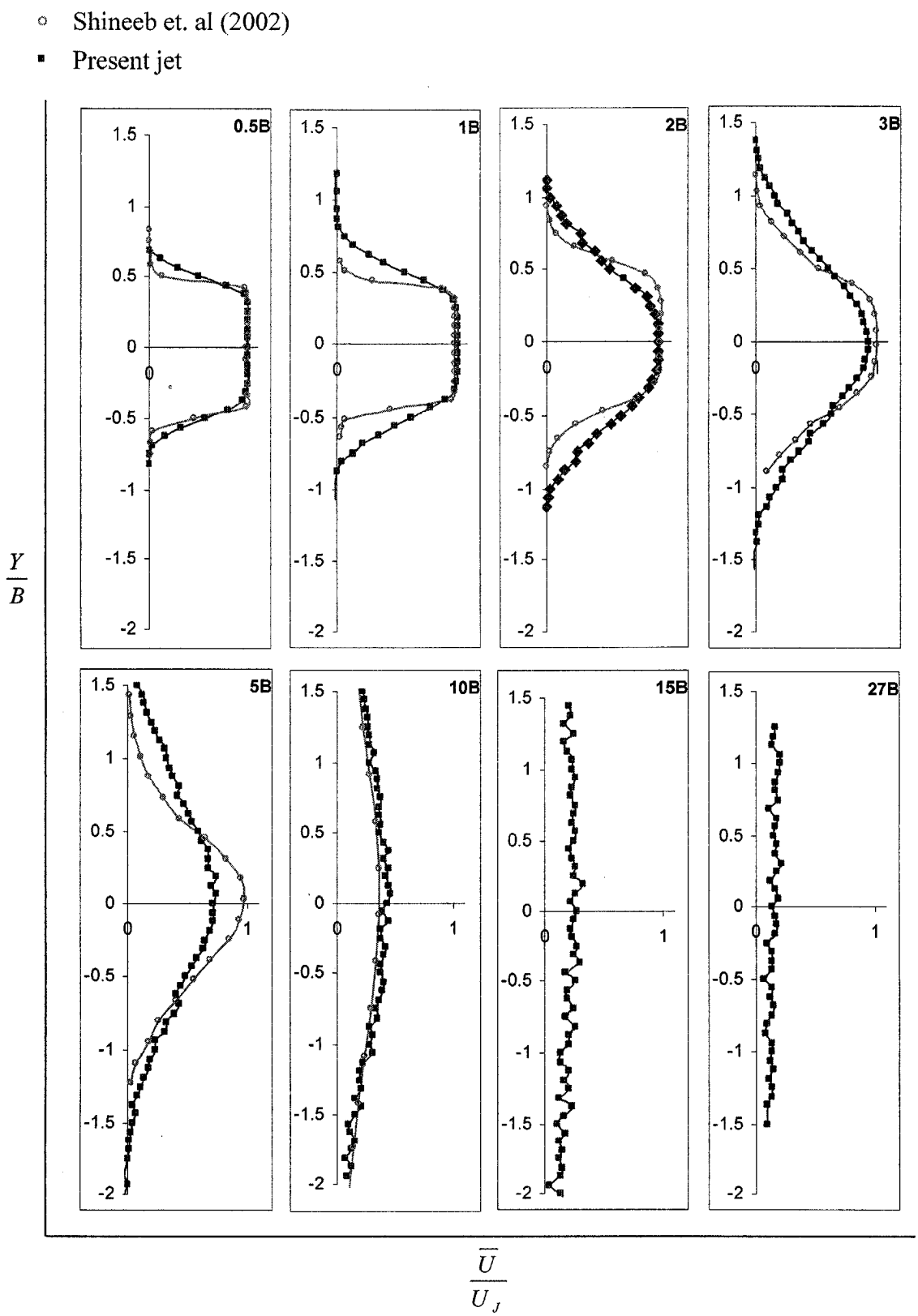

Figure 4.2: Streamwise mean velocity distribution at varying distances downstream

at the upper right hand corner of each of the graphs. A comparison is made between the present jet and with those of top-hat jets obtained by other researchers. The high quality PIV measurements obtained in a round free jet (Shineeb et. al., 2002) are plotted at various locations to enable a comparison with the present study. The open round symbols indicate the data set of Shineeb et.al(2002) while the closed square symbols indicate the present square jet results.

At the very first station, X/B = 0.5, the mean velocity distribution resembles a typical top hat profile. The nozzle width B and the jet exit velocity U_j are used as the normalizing scales. This graph also serves to illustrate the quality of the flow exiting the nozzle. The top-hat profile was set as a criteria for comparing the present data with the data available in the literature. Detailed description of the velocity profiles at other lateral locations are provided later.

In the middle 65% of the flow, the velocity is constant at 1 m/s. In the present investigation, evaluation of the first three graphs in Figure 4.2 indicates that the region of constant velocity in the central portion of the jet gradually decreases and the existence of the potential core region is seen upto X = 2B. The top hat velocity distribution gradually changes with increasing X/B and at X/B = 3, it resembles the Gaussian distribution as noticed in other axi-symmetric jet studies. Importantly, the change over from a top-hat profile to a Gaussian type occurs earlier than that noticed in a free axi-symmetric jet. It can be noted from the profiles that the square jet has expanded more than the round free jet. The present results at X/B = 3 also indicates axi- symmetric distribution. As we proceed to the next station X/B = 5, the shape of the profile changes. As a consequence of the jet impinging on the free surface it can no longer expand in this direction. In the

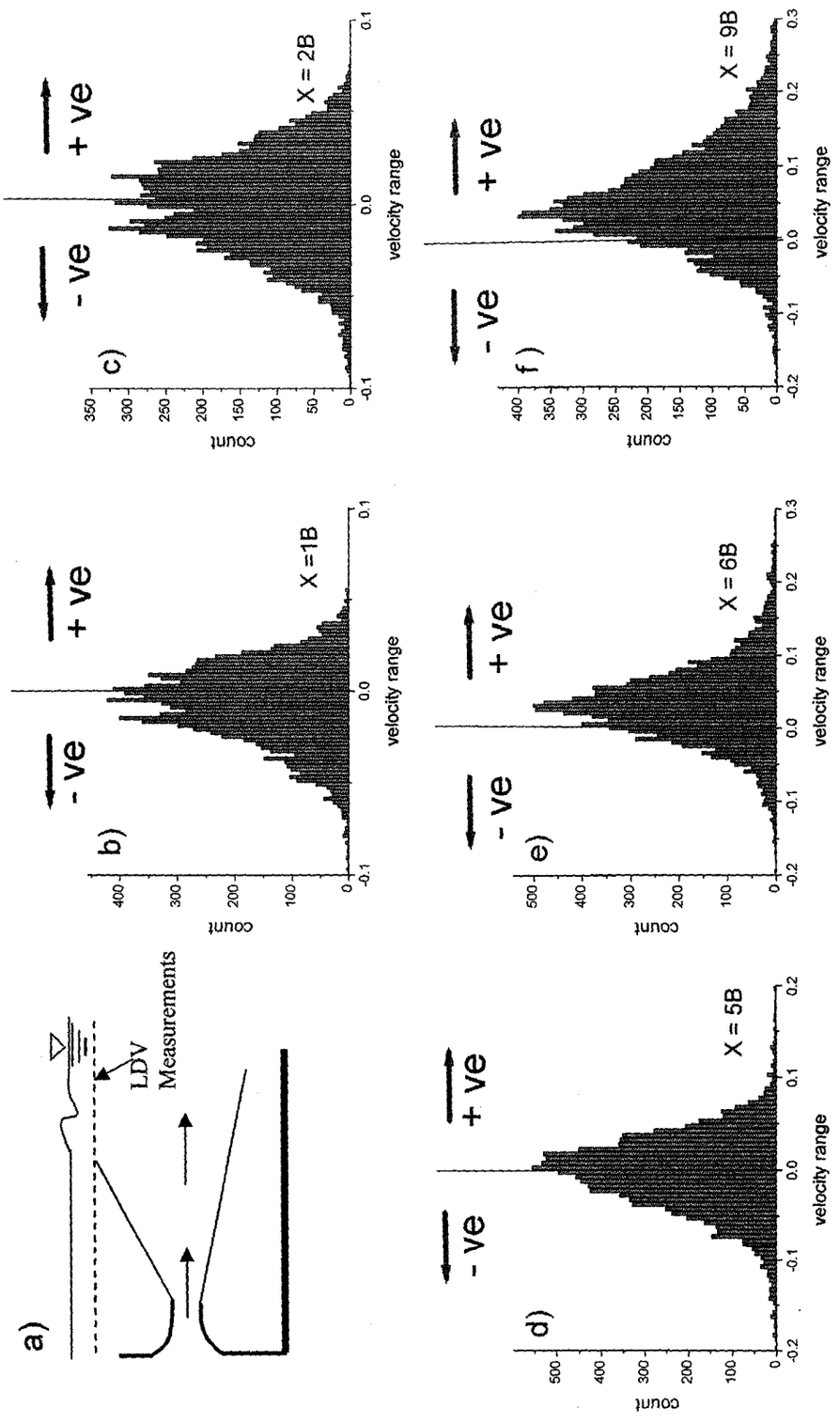

4.3: Velocity Histogram

bottom half, the jet expands in a manner that has been traditionally noted in free jet studies as the jet has not yet directly interacted with the bottom wall.

In an effort to identify the impingement point on the free surface, velocity histograms for varying downstream distances are plotted. The measurements were made 0.01m below the free surface (Figure 4.3 a). A criterion based on equal distribution of positive and negative velocities in the histogram will indicate this impingement point. Figure 4.3 shows the streamwise velocity histogram for various downstream distances. The corresponding stations are marked on the right hand bottom corner. Regions before jet impingement are expected to have dominant negative velocities because of the reverse flow in the recirculation zone (Figure 4.1 d). At X = 1B, 60.5 % of the mean velocity is negative, indicating a strong reverse flow. As we proceed to the next few stations, one can notice that there is a gradual reduction in the proportion of negative velocities. However it is important to note that there are negative velocities even at X = 9B. This provides an indication of the region over which the jet impinges on the free surface causing the local motion to be unsteady. Careful observations indicate that one can visually define a mean impingement point around X = 4B and conforms to the velocity measurements.

In terms of a boundary, the free surface could be considered to behave like a 'weak' wall owing to surface tension effects (Nezu, 2005). Following jet impingement, the fluid particles near the free surface starts to move along the streamwise direction which in turn affects the symmetrical distribution of the mean streamwise velocity profiles. The confinement effects due to the presence of the free surface cause higher velocities at symmetrical locations on either side of the nozzle axis. For example, in Figure 4.2, at

X/B = 5 and Y/B = +1 the velocity is about 0.3 m/s while at X/B = 5 and Y/B = -1 the velocity is 0.23 m/s. A close observation of the profiles at X/B = 5, reveals that the bottom part of the profile jet still resembles that of a free jet, whereas the profile near the free surface has changed. Progressing to X/B = 10, the jet gradually loses its form and one can clearly note higher velocities in the upper regions of the jet at compared to equivalent distances along the lower half of the jet. Close observation of the last two mean velocity profiles indicates a shifting of maximum velocity towards the free surface. At these last two stations the jet completely loses its form and one can note a mild velocity gradient with lower velocities at the bottom and higher velocities on top of the centreline.

As the jet evolves forming a shear layer envelope, the region outside the envelope is expected to have small velocities while the region inside has dominant positive velocities. The difference in the velocity between the jet and the ambient fluid results in entrainment which slows the jet causing velocity to decay.

Table 3. Comparison of velocity decay rates and kinematic origins for jets.

Jet Type	Range	Velocity decay rate (K_d)	Kinematic Virtual Origin (C_k)
Square free jet (Quinn and Militzer, 1992)	$8.4 \leq X/D_e \leq 62.4$	0.185	-0.15
Round free jet (Wygnanski and Fielder, 1969)	$10 < X/D > 50$	0.169	-3.0
Square jet (present jet)	$5 < X/D_e < 27$	0.200	0.07
Round free jet (Shineeb et. al, 2005)	$10 \leq X/D_e \leq 50$	0.170	-0.98

A curve of the form $\frac{U_j}{U_0} = K_d(\frac{x}{D_e} + C_k)$ is commonly used to describe the decay rate. Here, U_0 is the centreline velocity at any given station, D_e is the diameter (equivalent diameter of the square slot), K_d is the decay rate and C_k is the virtual origin.

Table 4.1 shows a comparison of decay rates and virtual origin. From Table 4.1, it is evident that the present square jet is decaying at a higher rate, i.e., the jet spreads more with higher entrainment of ambient fluid.

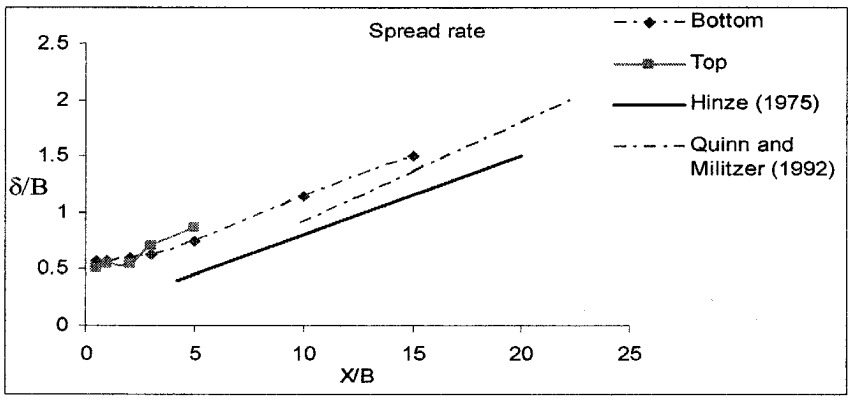

Figure 4.4: Half - width variation

The variation of the jet half – width (δ) with distance from the nozzle is shown in Figure 4.4. The half - width for the upper half of the jet is shown separately from the lower half. For comparison, the half width variation for a conventional round jet (Hinze, 1975) and a free square jet (Quinn and Militzer, 1992) is also shown in Figure 4.4. No corrections for geometric virtual origin is provided in Figure 4.4 and comparisons are linked to the slope of the curves. Clearly, the square jet has a higher spread than both free and round jets. In the present study, the top and bottom spread rates are similar for X/B < 5. Furthermore, the slope of the line in the present far field data (X/B >5) is 0.080

4.2 Turbulence Characteristics

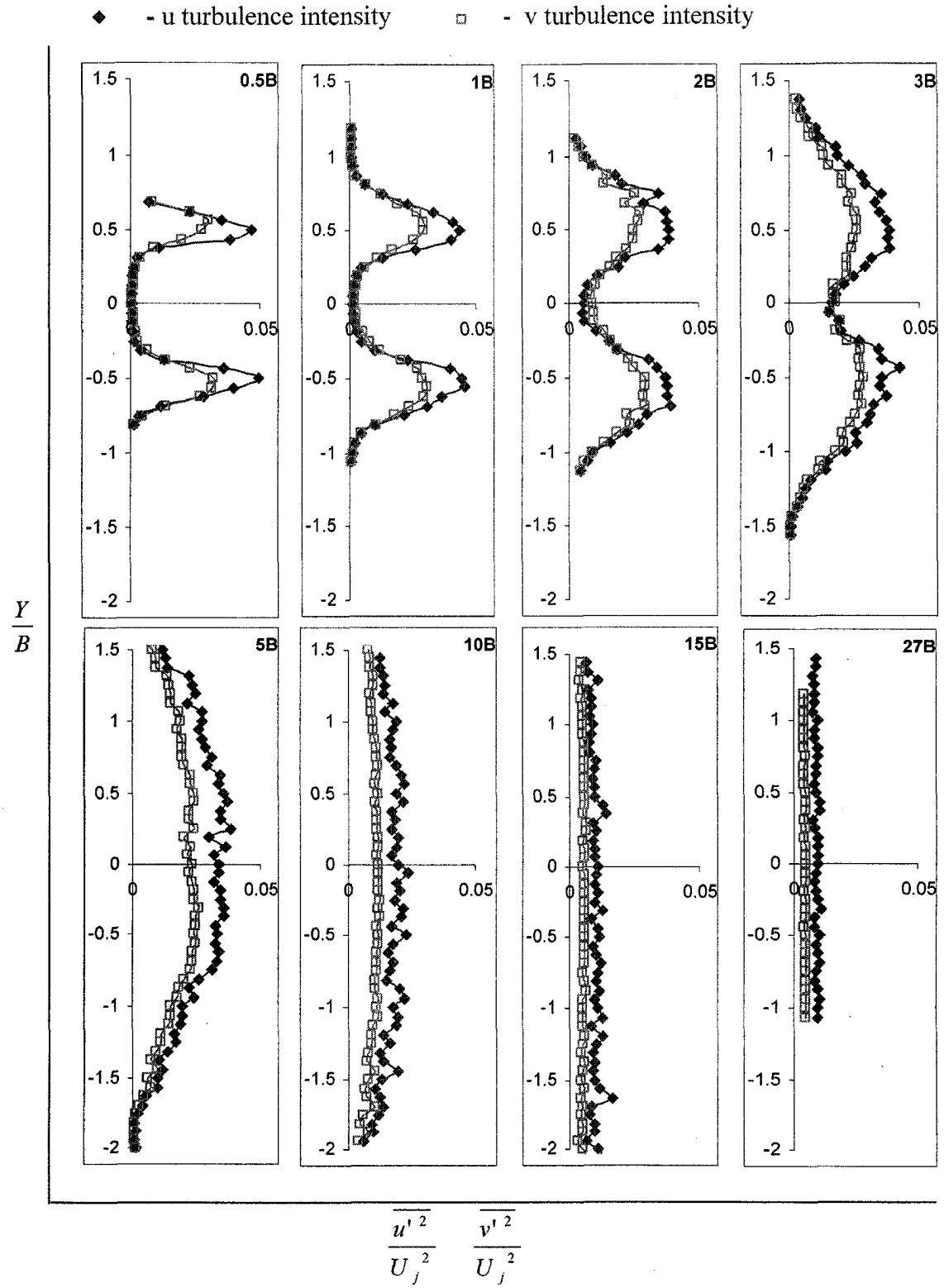

Figure 4.5: Streamwise and Normal turbulence intensity profiles at various downstream locations

which is similar to the value observed by Hinze (1975). However, the spread rate observed for square free jets by Quinn and Militzer (1988) is higher. It should be noted that the jet of Quinn and Militzer (1992) is not influenced by a free surface and hence can.entrain more ambient fluid. One can expect a decreased entrainment from the top region of the present jet due to confinement effects.

Figure 4.5 shows the downstream evolution of streamwise and normal turbulence intensities. At the very first station (X/B = 0.5), distinct double peaks are observed. This is due to the enhanced turbulence activity at the edges of the jet while the central portion of the jet has no turbulent activity (potential core region). Also, one can clearly note that the streamwise turbulence intensity is greater than the normal turbulence intensity at the peaks denoting anisotropic conditions. At X/B = 2, there is a decrease in the turbulence intensity at the edges as the streamwise fluctuations are suppressed due to the entraining fluid. The turbulence intensity at the centre is no longer zero and it begins to increase with increasing distance downstream as the core region begins to perturb. At X/B = 3, a close observation reveals that the peaks are spread out and a range of values close to the maximum intensity are noted as opposed to a single peak at X/B = 0.5. The peaks observed at X/B = 3 occupy about 20% of the nozzle width on either sides of the jet centreline. At the next station (X/B = 5), the double peak disappears indicating intense mixing. After interacting with the free surface (X/B = 5 and X/B = 10) there is a slight increase in the streamwise and normal turbulence intensity profiles closer to the free surface compared to identical locations at the bottom of the jet. At X/B = 27, the profiles straighten out and the intensity is distributed evenly throughout the jet due to momentum diffusion.

In the first three sections namely X = 0.5B, 1B and 2B of the mean velocity profile, u turbulence intensity, v turbulence intensity, it appears that the profiles are different from that of a traditional free jet. The next three stations, X = 3B, 5B and 10B are quite different from the free jet, typical ZFE (zone of flow establishment) for a round jet is between 10B and 15B from the nozzle, ZEF(zone of established flow) is about 20B from nozzle. The present case is different, the flow changes characteristics quite differently from 5B to 27B and one can see that the jet has completely diffused by 27B.

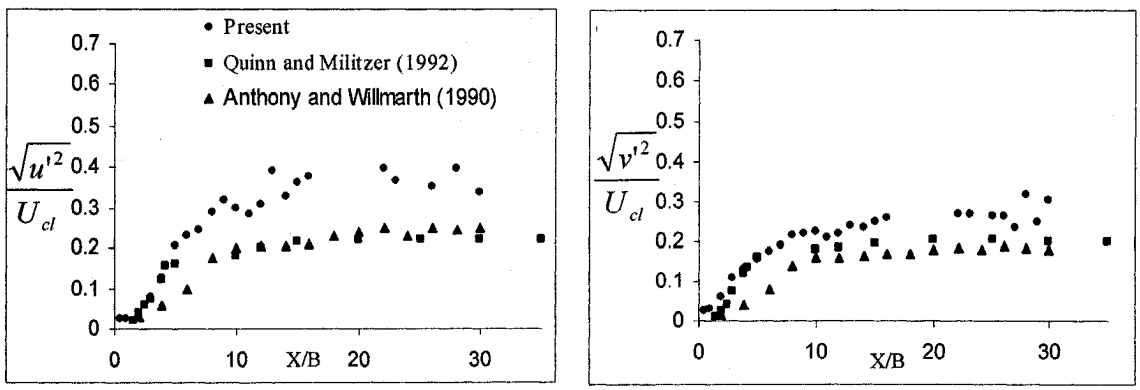

Figure 4.6: Variation of streamwise and normal turbulence intensities along the centreline.

Figure 4.6 shows the streamwise and normal turbulent intensity variation along the jet centreline. The fluctuations are scaled by the streamwise mean velocity at the centreline at corresponding downstream locations. It can be noted that there is a steep rise in the turbulence intensities in the initial region. In the region X/B >10, the streamwise fluctuations fail to stabilize to a constant value as in the case of a free square jet (Quinn and Militzer, 1992 and Anthony and Willmarth, 1990. Wygnanski and Fielder (1969) found the constant value to be 0.29 for a turbulent free jet. This unstable rms fluctuation is due to the jet impingement on the free surface and increased confinement effects.

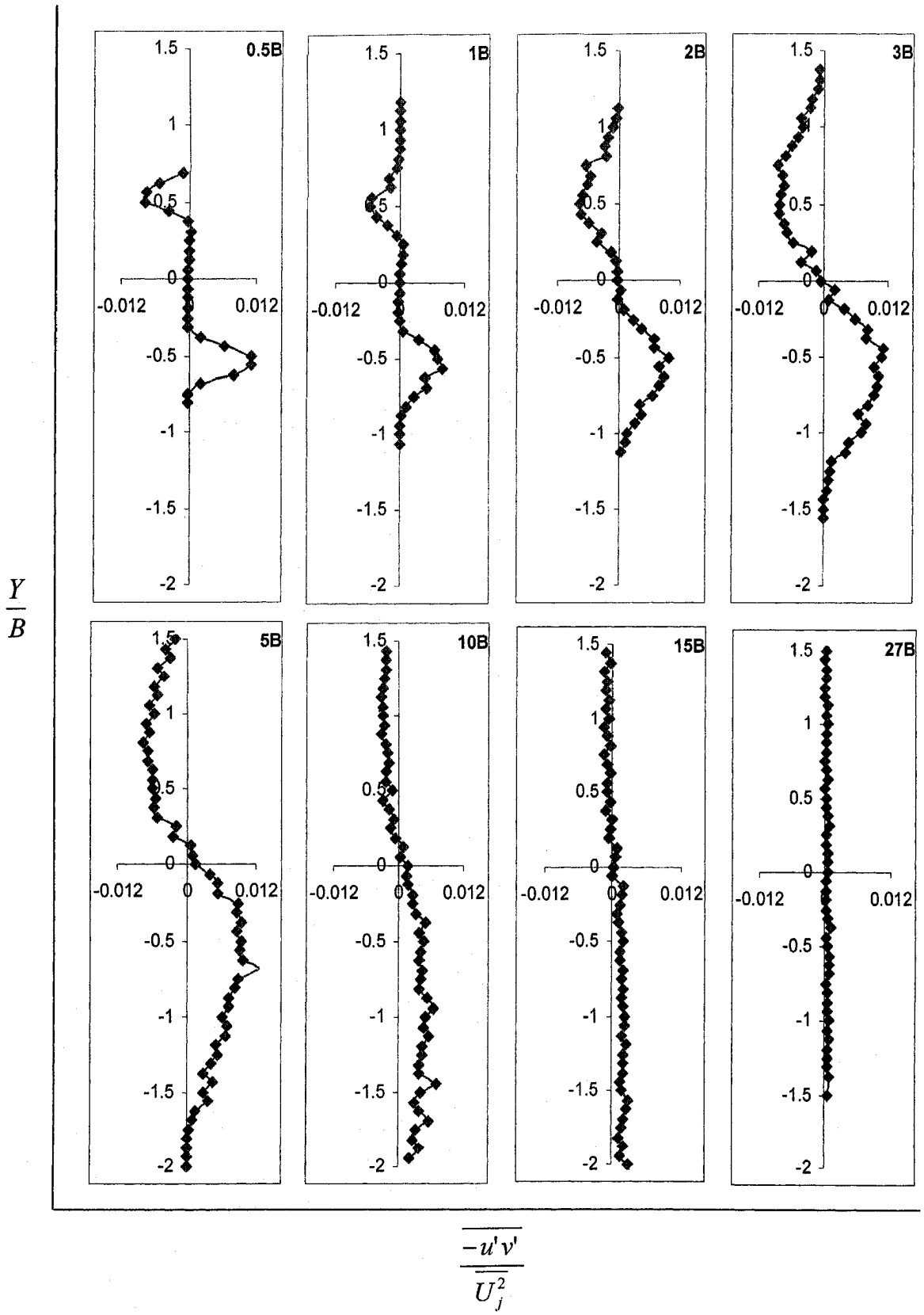

Figure 4.7: Shear stress evolution at various downstream locations

The interaction of the jet with the free surface has led to the generation of waves near the jet centerline. A similar behavior is observed in the normal turbulence intensity plots. The streamwise fluctuations are higher than the vertical fluctuations rendering the flow to be anisotropic.

Figure 4.7 shows the shear stress profiles for increasing distances downstream of the nozzle. At X/B = 0.5, distinct double peaks are observed, a negative peak at Y/B = +0.5 and a positive peak at Y/B = -0.5. The profile is nearly antisymmetric about the centreline. On either side of the centreline the jet flow is outward, corresponding to an outward growth of shear, whereas near the edges entrainment causes an inward flow and hence an inward shear. The absolute value of the peak at the bottom is slightly higher than the peak at the top and is possibly due to the difference in the strengths of flow entraining into the jet from the top and bottom. Shear at the centre of the jet is zero and confirms the existence of the core region. The zero shear region extends to about 60% of the nozzle width. Similar behavior is noticed at X/B = 1 and X/B = 2 with the zero shear region extending to about 50% and 10% of the nozzle width, respectively. This is an indication of a decrease in the width of the core region with increasing distance downstream. At X/B = 5, the peak value of shear stress is shifted to Y/B = $\pm$ 0.8 at X/B = 5 from Y/B = $\pm$ 0.5 at X/B = 0.5 indicating that the jet has expanded. Following jet impingement on the free surface, one can clearly note a difference in the behavior above and below the jet centreline. The portion of the jet near the free surface (above the centreline) has lower values of shear stress to comparable locations below the jet centreline. This is due to the influence of the free surface which cannot sustain shear stress. Progressing further, to X/B

= 10 and 15, the free surface effects are seen to penetrate into the jet. The peaks have disappeared, the shear stress above the centreline is zero while the shear stress below the centreline is significant. The portion of the jet above the centreline loses the jet like behavior while the portion below the jet centreline still retains features of the jet. Thus different dynamics at free surface (zero stress) compared to the solid wall (zero velocity) are observed in confined jets. At X/B = 27, the profile is a straight line and the jet has completely diffused.

One can visualize a mixing ring formed along the periphery of the jet between the potential core and the outer region of expansion of the jet. In terms of shear, the mixing zone is quite different at the very first station, for example, X/B = 0.5, one can see that the mixing zone is small, noted from the spread of the peaks at Y/B = +0.5 at the top. The width of the mixing zone is 0.3 B at the top. A similar zone can be noted at the bottom corresponding to Y/B = -0.5, the width of the bottom affected zone is 0.45 B. One can clearly note the increased mixing zone at the bottom due to enhanced entrainment. The mixing zone is seen to increase with increasing distance downstream. At X/B = 3, turbulence has penetrated the potential core with the mixing zone extending throughout the jet.

4.3 Higher order moments

In the following section the higher order velocity moments are discussed. In Figure 4.8, each of the horizontal rows represent the evolution of a single variable. The variables of interest include $\overline{u^2v}$, $\overline{u^3}$, $\overline{v^2u}$ and $\overline{v^3}$. All the variables discussed in Figure 4.8 are normalized by U_J^3. The corresponding length scale is the nozzle width.

A need to understand the behavior of coherent structures has triggered the study of triple correlations. Turbulent events like bursts, ejections, sweep etc have been identified in wall bounded flows. A measure of these events can be obtained from the higher order moments. A similar analysis is adapted in the present study. These events and the corresponding higher order moments provide information on the coherent structures in the flow. Salient features of turbulent events like ejection, sweep etc., cannot be studied using the mean and the turbulence intensity profiles. An effort is made to freeze the flow by subtracting the mean and study the role of velocity fluctuations. This approach is similar to the boundary layer studies.

Turbulent diffusion of $\overline{u^2}$ in the y direction can be thought of as $D_v = (\overline{u^2v})$. Row 1 in Figure 4.8 corresponds to $\overline{u^2v}$ at different downstream locations. Discussions are presented at X/B = 0.5. For this station, D_v is zero in mid 60% of the flow. This corresponds to the observation in the mean profiles and denotes zero turbulent diffusion. The potential core region is similar as observed earlier in the mean and turbulence intensity profiles. At the edges of the jet there are two local peaks, one positive and another negative, whereas in the shear and turbulence intensity profiles there is only one peak observed. A positive value of $\overline{u^2v}$ indicates an upward transport of u momentum in the upward direction. At X/B = 0.5, Y/B = 0.63, a positive peak (peak A) is noted in

the $\overline{u^2v}$ profile. The motion of fluid parcels out of the jet in the form of ejecting eddies results in a positive peak in the $\overline{u^2v}$ profile at Y/B = 0.63. A review at the shear stress profile (Figure 4.7) at this location indicates no peak formation revealing the sensitivity of triple correlations to fluctuations in the velocity. At Y/B = -0.63 the fluid parcels are ejected down thereby transporting u momentum downwards and hence $\overline{u^2v}$ has a negative value (peak B). The absolute value of the peak at Y/B = 0.63 in the $\overline{u^2v}$ plots is smaller than the value at Y/B = -0.63. This is a consequence of the ability of the jet to transfer more u momentum downwards at the bottom of the jet. The difference in the magnitude of the two peaks (A and B) is possibly a consequence of the difference in the boundary condition. The negative peak in the $\overline{u^2v}$ plot at Y/B = 0.43 (peak C) is consequence of entering eddies, because of the fluid parcel is being pulled down and into the jet. The positive value of ($\overline{u^2v}$) at Y/B = -0.43 (peak D) denotes that the fluid parcel is pulled above or ejected into the jet possibly because of entrainment from the bottom and resulting in upward transport of u momentum. The difference in the magnitudes of the peak indicate differences in the prevailing entrainment characteristics.

The magnitude of the positive and negative peak at Y/B = 0.63 and Y/B = 0.43 are almost the same which implies that on an average the entering eddies and the ejection eddies will cancel out. However, at the bottom the, diffusion component of the entering eddies are stronger than the ejection eddies as seen from the slightly increased peak at Y/B = -0.43 (peak D). Further analysis on this region is provided in the forth coming section of quadrant decomposition.

It is noted in the $\overline{u^2 v}$ plots, comparing peaks C & D, the fluid entrainment into the jet in the bottom is higher than the one at the top i.e. absolute values of the peaks at Y/B = -0.43 is greater than the value at Y/B = 0.43. This behavior has been noticed in all the tests conducted in the present study. This signifies that there are stronger entering eddies from the bottom of the jet compared to the top. Further, entrainment from the bottom is slightly higher than the entrainment from the top which is possible due to the higher extent of ambient fluid at the bottom of the jet. At X/B = 0.5, the values of ($\overline{u^2 v}$) above Y/B = 0.63 and below Y/B = -0.63 are close to zero and does not contribute to the turbulence characteristics.

The diffusion characteristics at X = 1B is similar to that noticed at X = 0.5B. As we progress to X = 2B, there is a slight increase in the magnitude of the negative peaks (peak C) in the $\overline{u^2 v}$ plots at the top of the jet as compared to the value at X/B = 0.5 and 1.0. This is due to the increase in the strength of the entering eddies. The location of the negative peak above the jet has shifted from Y/B = 0.43 at X/B = 0.5 to Y/B = 0.38. This is a result of turbulence penetrating the jet. A similar behavior is observed at the bottom of the jet. The tendency to entrain more fluid parcels from the bottom is still predominant and is observed in the increased negative peak (peak B) at Y/B = -0.38 from the $\overline{u^2 v}$ plot. It appears from peak D, that the strength of the entering eddies at the bottom is decreasing with increasing downstream distance.

At X = 3B, we can see a significant reduction in turbulence activities, there is little difference in the top and bottom peaks indicating that the strength of the entering eddies is the same. The plots look antisymmetrical on either sides of the jet centreline. At X = 5B, the jet impinges the free surface and loses the antisymmetrical distribution of the

turbulence quantities. The magnitude of the negative peak of $\overline{u^2v}$ at Y/B = -1.3, is greater than positive peak at Y/B = +1.3 which would mean that the jet is ejecting stronger eddies into the ambient fluid at the bottom, thereby transporting more streamwise momentum in the bottom. The strength of the entering eddies on either sides of the jet centreline have same magnitudes. At X = 10B, increased turbulence activity can be seen at the bottom of the jet from the relatively higher peaks at the bottom. The bottom of the jet is not directly influenced by the interaction of the jet with the free surface and it still exhibits jet characteristics, while the free surface has dampened the $\overline{u^2v}$ values above the jet centreline. At X = 15B and X = 27B, the distribution have straightened and the jet has completely lost its form.

Streamwise flux of streamwise momentum can be considered as ($\overline{u^3}$). Row 2 in Figure 4.8 corresponds to $\overline{u^3}$ at different downstream locations. At X/B = 0.5 and Y/B = ± 0.63, positive peaks are observed, this is due to the ejecting eddies which are ejected out from the jet. At Y/B = ± 0.43, negative peaks are observed indicating entering eddies which are pulled into the jet due to entrainment. The positive and negative peaks above the jet centreline have comparatively lower strengths than the peaks observed below the jet centreline. This is possible because of the slightly enhanced eddy transport at the bottom due to the higher extent of ambient fluid. A cross-over point in the profile is observed at the region of high shear (Y/B = ± 0.5).

At X = 2B, a similar behavior is observed with the entering eddies stronger than the ejecting eddies. The location of the negative peak above the jet has shifted from Y/B = 0.43 at X = 0.5B to Y/B = 0.375 at X = 2B and the location of the negative peak below the jet centreline has shifted from Y/B = -0.43 at X = 0.5B to Y/B = -0.375 at X =2B

indicating a clear decrease in the width of the potential core region. At X = 3B, one can observe that the negative peaks on either sides of the jet centreline are close to each other. The value of $\overline{u^3}$ at the centreline is beginning to increase indicating penetration of turbulence. Following jet impingement, At X = 5B, the negative peaks have merged with a maximum value at the centreline. The profile below the jet centreline has higher values to comparable values above the jet centreline, indicating the greater strength of the ejection eddies at the bottom of the jet. At X/B >15 the profile does not indicate any jet like behavior.

Turbulent diffusion of (v^2) in the x direction can be thought of as ($\overline{v^2 u}$) = Du, ($\overline{v^3}$) can be considered as the normal flux of v momentum. Row 3 and row 4 in Figure 4.8 correspond to the $\overline{v^2 u}$ and $\overline{v^3}$ profiles at different downstream locations. These profiles follow a similar trend as observed in $\overline{u^3}$ and $\overline{u^2 v}$ respectively.

At X/B = 5, referring to all the profiles in the column, we note that D_v and $\overline{v^3}$ are not as symmetrical as D_u and $\overline{u^3}$. Obviously, the presence of a free surface influences the v component (suppression) and is clearly reflected in these profiles.

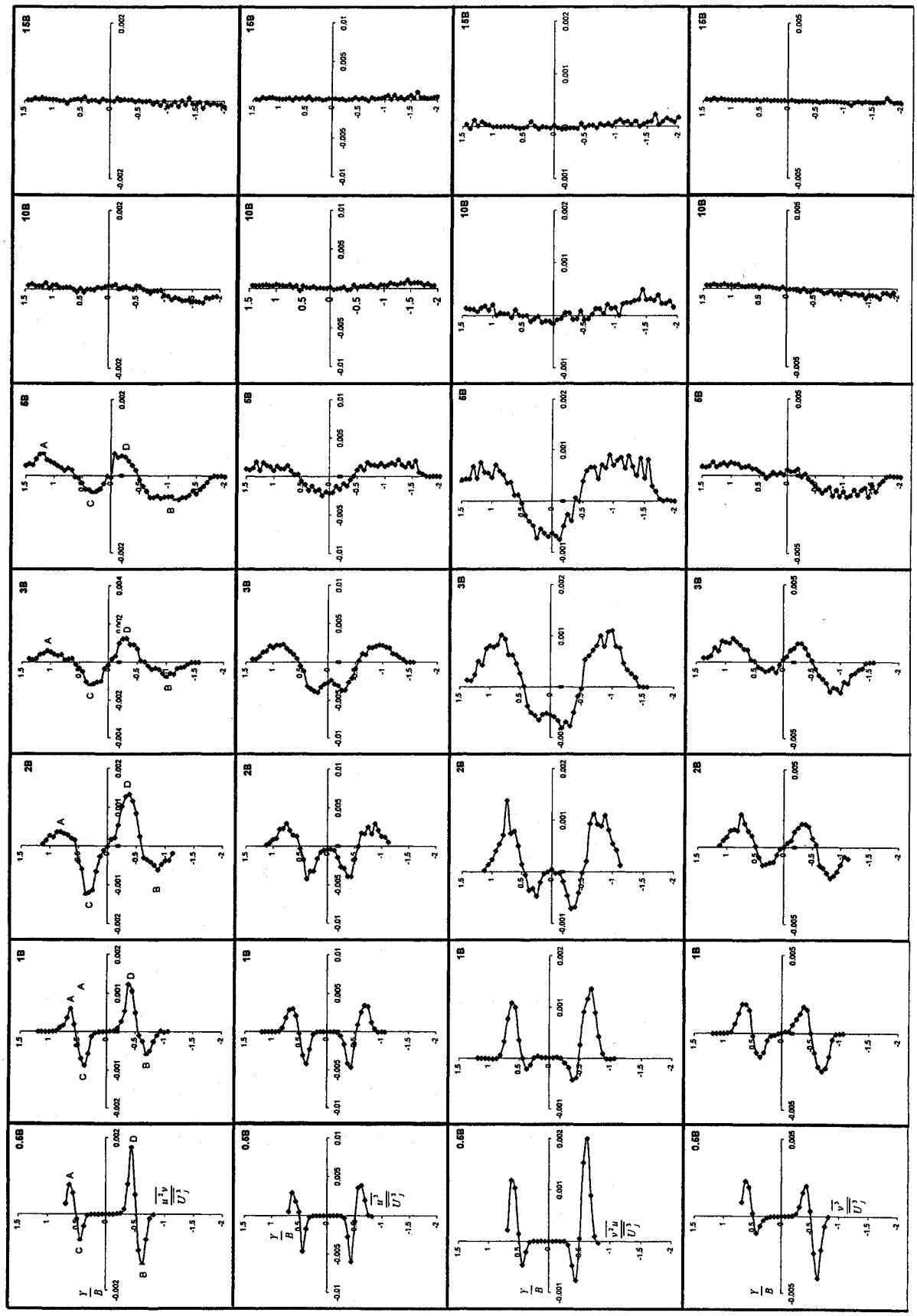

Figure 4.8: Evolution of higher order moments at different downstream locations

4.4 Quadrant analysis

The higher order triple correlations considered earlier provide useful information, but some aspects related to sign (+/-) are lost. For instance, the term u^2v could be positive as a result of v being positive and u being positive or negative. Furthermore, averaging the data (i. e, $\overline{u^2v}$) results in further loss of information. Quadrant analysis provides for an analysis where the contribution of velocity fluctuations retain sign information that can assist in distinguishing turbulent structures.

The instantaneous velocity vector at any given point is resolved into streamwise and normal components from which fluctuating components are calculated. A plot is made of the fluctuating components with u and v as the x and y axis. By doing so, the velocity fluctuations are decomposed into four quadrants as shown in Figure 4.9. The shear stress production in each quadrant can now be analyzed. Each data point in any given quadrant can be considered to be a result of a turbulent event. In order to distinguish background turbulence from those generated by large scale events, each of the events is further distinguished into a hole region and an extreme event region by defining a rectangular hyperbola (Figure 4.9 a). For conditional sampling of the LDV data, Lu and Willmarth, (1973), developed a detection function F(n) with the help of a hyperbolic hole size, H defined by $|uv| = H u' v'$ (where u' and v' are rms values).

$$\text{F (n)} = \begin{cases} 1 \ when \left| uv \right|_Q \geq H u' v' \\ 0 \ otherwise \end{cases}$$

The data below the threshold value is said to be in the hole and correspond to quieter periods. The threshold lines defined by $|uv| \geq H u'v'$ are used to denote extreme events. The larger contributors can be extracted leaving the smaller fluctuations in the hole.

Figure 4.9 b shows a schematic of a flow field with four different eddies denoted as A, B, C and D. Though fluid motion occurs in all the directions, for

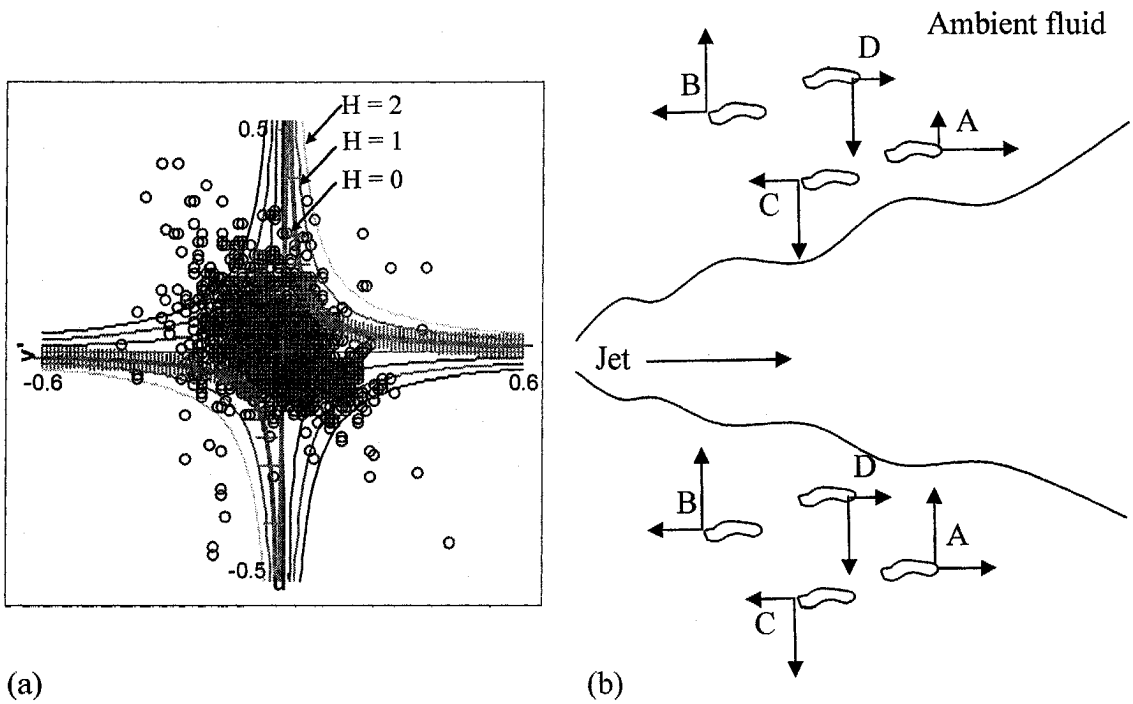

Figure 4.9: Quadrant decomposition

simplicity four kinds of eddies are shown. As noticed earlier, the behavior of eddies above and below the jet centreline is different. To better understand the eddy motion, their movement above the jet centreline is discussed. Eddy 'A' corresponds to a particle with a large value of u and a small value of v; would correspond to a particle being swept away. Eddy 'B' denotes a slow moving particle in the streamwise direction that is exiting the jet. Eddy 'C' and eddy 'D' by virtue of the arrows, indicate a fluid particle entering the jet. The fluid eddies A, B, C and D in Figure 4.9 correspond to specific quadrants. Above the jet centreline, the fluid eddy A corresponds to a quadrant 1 (Q1) event. Similarly eddy B, eddy C and eddy D correspond to quadrant 2 (Q2), quadrant 3 (Q3) and quadrant 4 (Q4), respectively.

Figure 4.10 shows the shear stress in each of the quadrants for varying downstream distances (H = 0). Above the jet centerline, at X/B = 0.5, Y/B = +0.5, four significant peaks are observed of which quadrant 1 (Q1) and quadrant 3 (Q3) are dominant. Above the jet centreline, Q1 and Q3 correspond to exiting and entering eddies respectively. Below the jet centreline at Y/B = -0.5, four significant peaks are observed of which Q2 and Q4 are dominant. In brief, Q1 at the top of the jet is similar to Q4 at the bottom and they correspond to exiting eddies, Q3 event at the top portion of the jet is similar to Q2 at the bottom of the jet corresponding to entering eddies. Referring to the top portion of the jet, the identical peaks Q1 and Q3 may result in a canceling effect above the jet centreline as the void left by eddy A is filled by eddy C. Similarly the peaks Q2 and Q4 may result in a canceling effect below the jet centreline as the void left by eddy D would be filled by eddy B. The peaks at the bottom are comparatively higher to the peaks at the top and can be attributed to more turbulent friction losses at the bottom. At X/B = 0.5, the bottom peaks of Q2 and Q4 are 20% higher than the top peaks of Q1 and Q3.

It can be seen from the high value at peaks that the exiting and entering eddy behavior is predominant in the near jet region (X/B < 5). With increasing distance downstream, at about 5B the less significant peaks above and below the jet centreline disappear and hence do not contribute to the shear stress any further. It can clearly be seen that at 5B only 2 peaks are noted on either side of the jet centreline. Progressing further the peaks formed by Q1 and Q3 above the jet centreline and Q2 and Q4 below jet centreline diminish and disappear completely indicating that the jet has completely diffused.

As the value of H is increased to two, the data is indicative of stronger turbulent events. Figure 4.11 shows the shear stress in each of the quadrants for varying downstream distances (H = 2). There are only two significant peaks on either side of the jet centreline as opposed to four when H = 0, denoting that these peaks correspond to stronger turbulent events. The peaks of Q1 and Q3 above the jet centreline and the peaks Q2 and Q4 below the jet centreline do not correspond to similar locations as compared to their formation at corresponding locations for H = 0. A crossover point between the dominating peaks is observed at Y/B = ± 0.5. At X/B = 0.5, the peaks of Q3 and Q2 correspond to the location Y/B = +0.43 and -0.43 respectively and is indicative of individual fluid parcels being pulled into the jet (entering eddies). At Y/B = +0.625 and -0.625, Q1 and Q4 indicate that individual fluid parcels are thrown out (exiting eddies) from the jet. With increasing distance downstream the distance between the peaks increase and the jet completely loses its form at X = 10B.

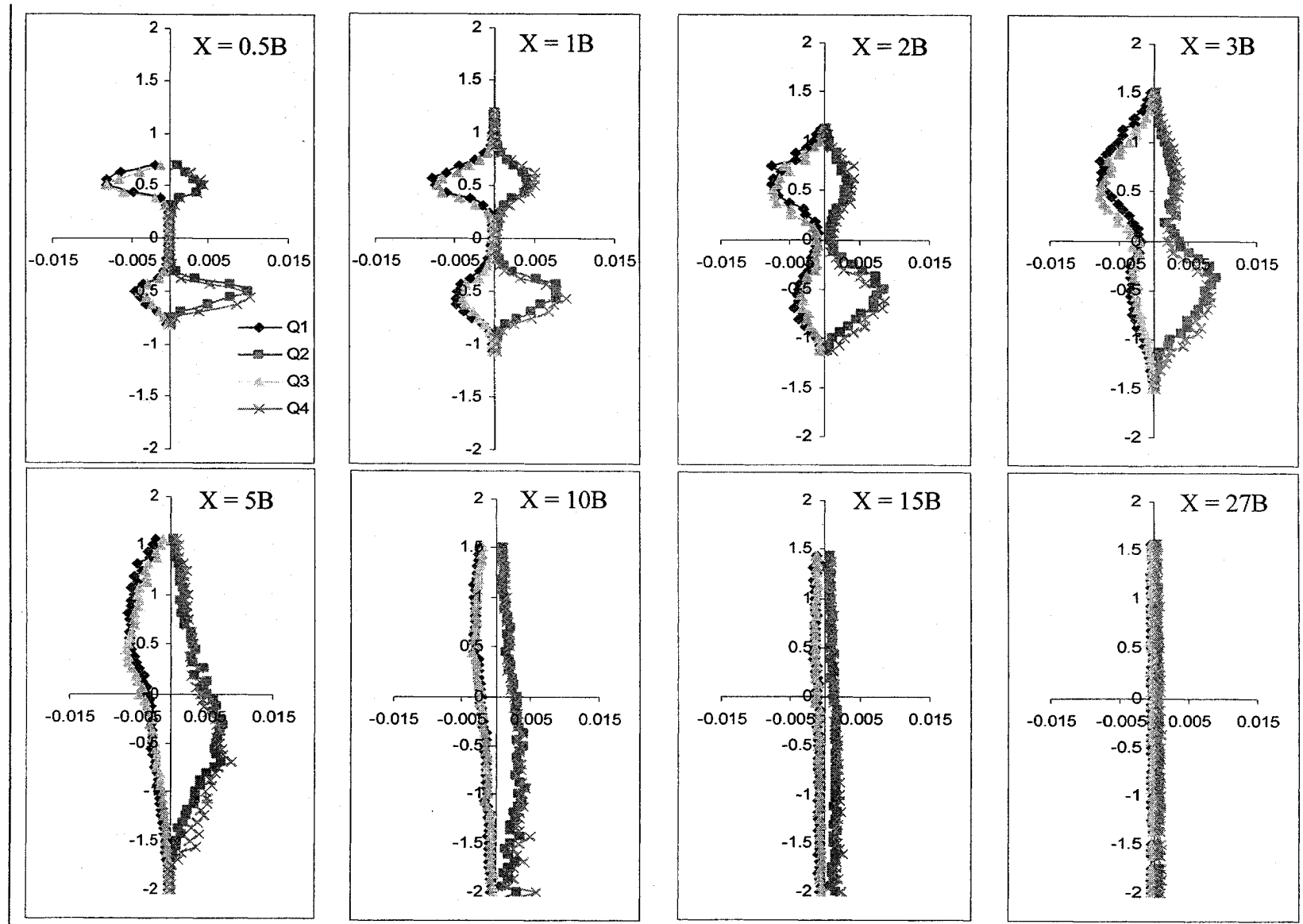

Figure 4.10: Shear stress contribution in each of the quadrants for varying downstream distances for H = 0

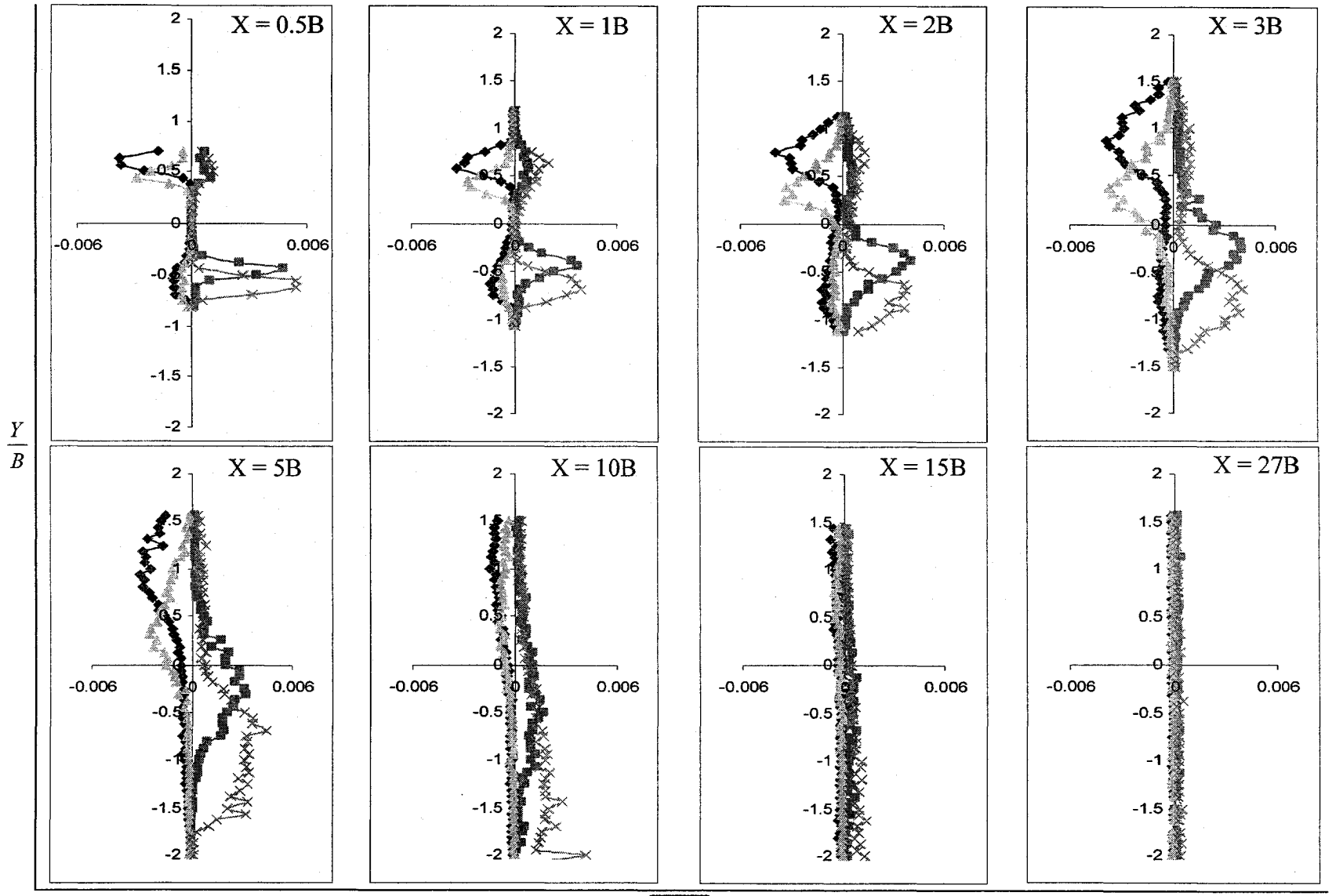

Figure 4.11: Shear stress contribution in each of the quadrants for varying downstream distances for H = 2

4.5 Axis - Switching in square jets

An interesting phenomenon called axis switching is responsible for the enhanced mixing that occurs in square jets compared with circular jets (Grinstein and DeVore, 1996). As the jet exits the nozzle, there is a region of high shear surrounding the jet. Vortices are formed along the perimeter of the square jet. Previous investigators Grinstein and DeVore (1996) have studied these vortices considering them to be a vortex tube moving with a velocity

$$u \approx \xi b \log(\frac{1}{\sigma})$$

Here, ξ is the local curvature of the tube, b the binormal to the plane containing the tube and σ is the local cross sectional area. Since the curvature of the vortex tube is more at the corners than the flat sides, the corners have a greater velocity than the flatter sides. This complex initial deformation of the vortex ring leads to the process of axis switching.

Transverse Velocity Profiles

In order to get an insight into the axis switching phenomenon, spanwise profiles at transverse locations along the width of the square nozzle was taken. Figure 4.12 shows the velocity profiles at three transverse locations. The transverse locations correspond to Z/B = 0, Z/B = 0.25 and Z/B = 0.5, Z/B = 0 corresponds to the measurement made at the jet centerline and Z/B = 0.5 corresponds to measurement at the edge of the nozzle. At a station X/B = 0.5, there is no major difference in the velocity profiles between Z/B = 0 and Z/B = 0.25. It can be clearly seen that the corners of the jet at location Z/B = 0.5, have peaks on either sides of the centreline. Also, there is a slight decrease in the

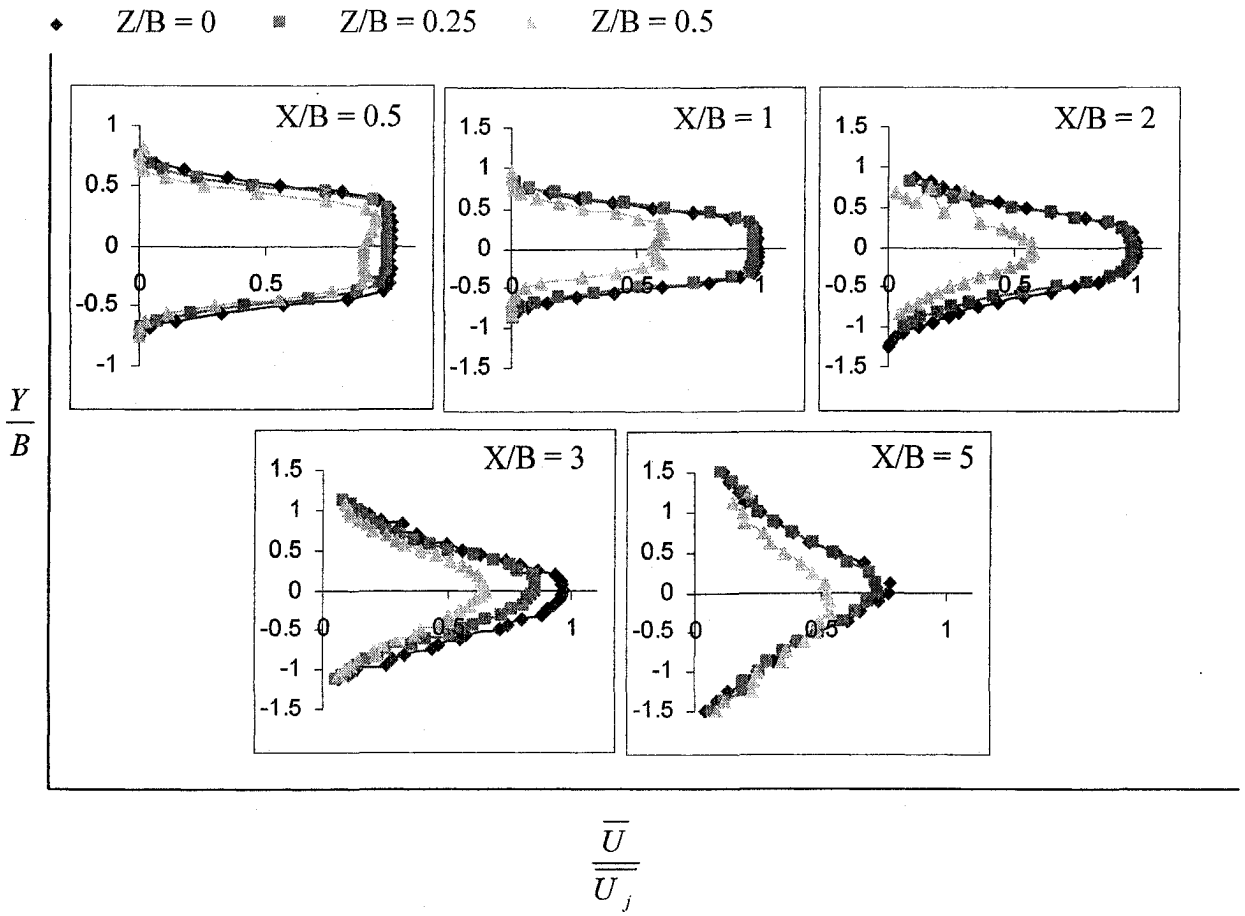

Figure 4.12: Spanwise profiles at tranverse locations

centreline velocity magnitude. At the station X/B = 1, the profiles at Z/B = 0 and Z/B = 0.25 are similar, there is a slight decrease in the width of the constant velocity region at the later location. At location Z/B = 0.5, there is a significant decrease in the centreline velocity and distinct peaks are observed on either sides of the centerline.

At X/B = 2, Z/B = 0.5, the double peaks have disappeared and the centerline velocity is 55% of the value observed at location Z/B = 0.25.

Greater mean velocity at the corners of the jet relative to the centreline values denotes the axis - switching behavior. This behavior is noticed up to 2B after which the square jet is thought to behave more like a symmetric jet.

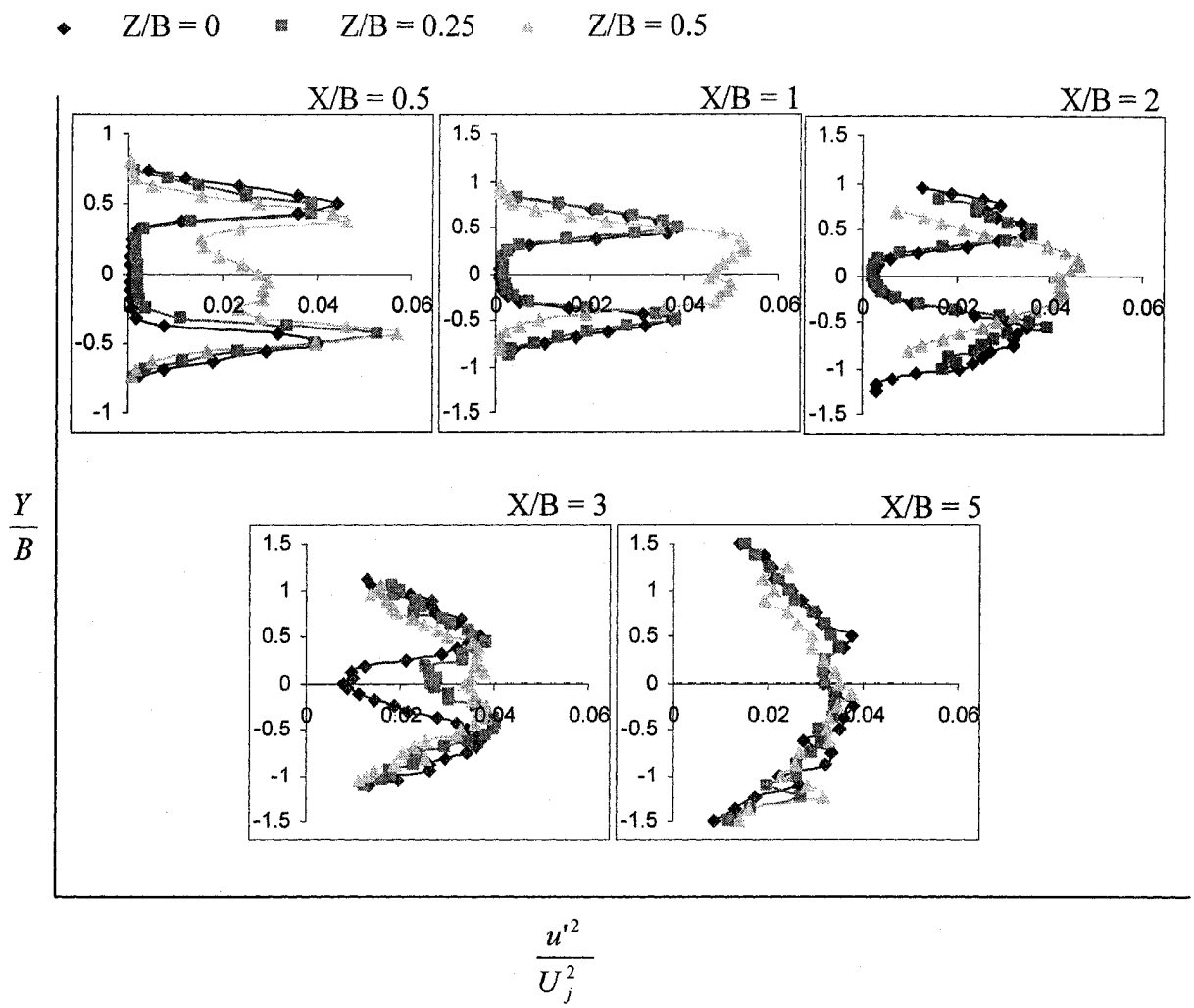

Figure 4.13: Streamwise turbulence intensity profiles at transverse locations

Figure 4.13 shows the variation of turbulence intensity profiles at the three transverse locations. It is seen in the very early region, X/B ≤ 2, the profiles at both Z/B = 0 and Z/B = 0.25 profiles follow a similar pattern with maximum intensity at the edges and zero intensity near the jet centerline. At X/B = 0.5 and Z/B = 0.5, the turbulence intensity at the centerline is higher due to the close proximity to the ambient fluid and entrainment from the sides. As the entrained flow further penetrates into the jet, the turbulence levels at Z/B = 0.5 continues to increase with increasing X/B. For X/B = 3, the

turbulence levels at Z/B = 0.25 is also increased and by X/B = 5, the entrained fluid has finally penetrated the jet.

4.6 Tailwater effect

This section compares and contrasts the behavior of the jet at different tailwater conditions used in this study. To recall, the four tailwater depths considered in this study are 1.5 B, 2.5 B, 3.5 B, 5 B measured from the bottom of the nozzle. For the tailwater of 1.5B the jet was seen to attach to the free surface soon after it evolved from the nozzle. For the other tailwater depths, the jet was observed visually to impinge the free surface at about X = 5B, 8B, 18B respectively. Figures 4.14 and 4.15 shows the distribution of various parameters at different distances downstream for all the four tailwater depths.

The first row in Figure 4.14 represents the streamwise mean velocity. The profiles are shown for four locations 0.5B, 2B, 5B, 10B, 15B. At a first glance, one may expect lesser decay rates at lower tailwater depths considering the fact that the amount of ambient fluid entrained should be much less than that at a higher tailwater depth. The mean velocity distribution at 1.5 B clearly indicates higher velocities compared to TW depth of 5B. The jet is observed to lose its symmetrical distribution eventually after jet impingement. For the tailwater of 5B the jet retains its symmetrical distribution even at the last measuring station whereas a tailwater of 1.5 loses its symmetrical distribution at about 10B and the maximum velocity starts to shift towards the free surface. The second and third rows in Figure 4.14 represent the streamwise and normal turbulence intensities. No significant differences can be noticed in the evolution of these profiles.

The fourth row represents the shear stress distribution. It can be clearly seen that for shallower tailwater depths of 1.5B and 2.5B the absolute value of the peak at the bottom is slightly higher than the peak at the top. As the tailwater depth increases i.e for 3.5B and 5B this difference in the peaks is not observed and can be attributed to the

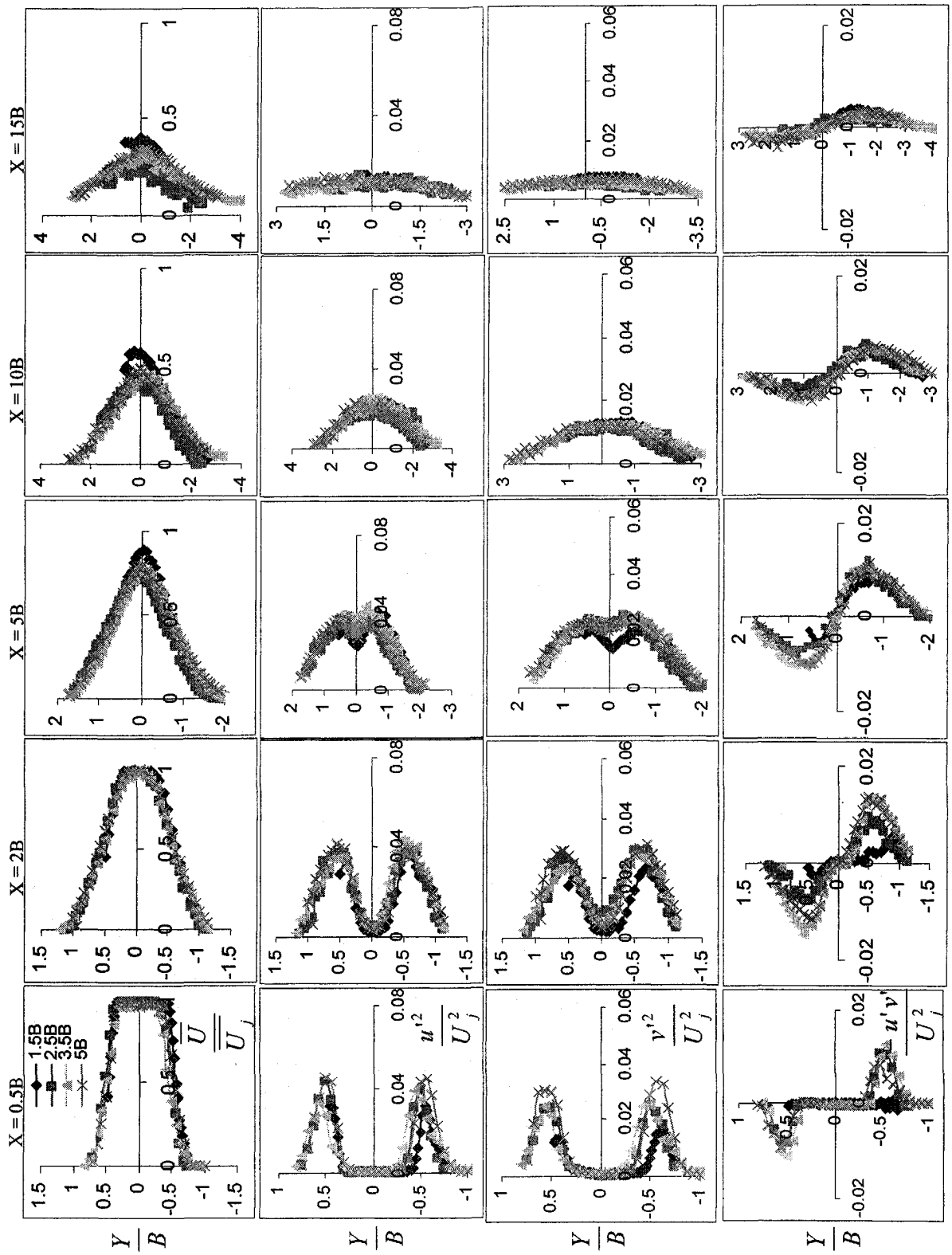

Figure 4.14: Distribution of mean, turbulence intensities, shear stress at different distances downstream for the four tailwater depths

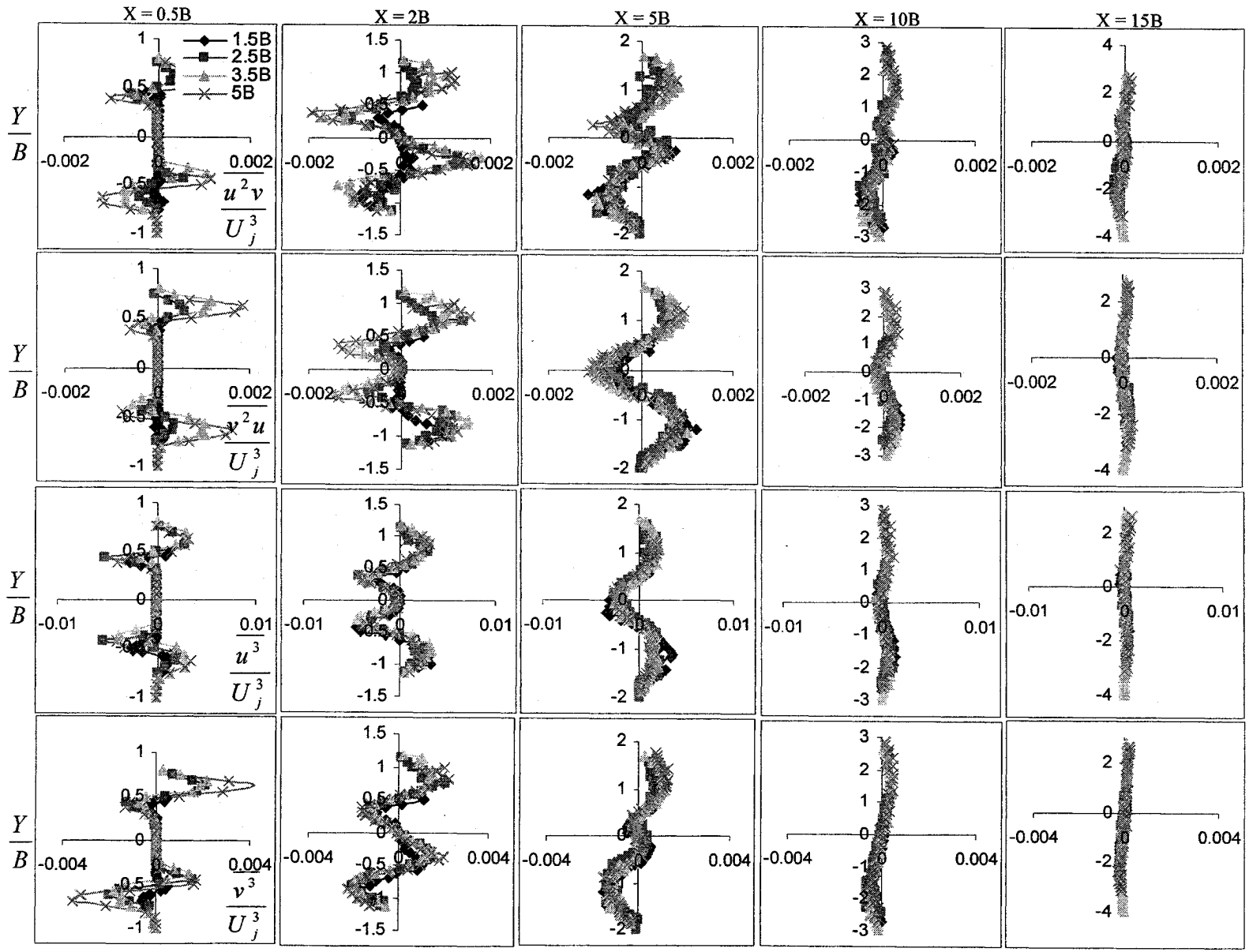

Figure 4.15: Distribution of higher order moments at different downstream locations for the four tailwater depths

extent of ambient fluid above the jet centreline and the proximity of the jet to the free surface (zero shear stress).

Figure 4.15 shows the diffusion coefficients at various tailwater conditions. The trends and the evolutions are very similar at all conditions.

Surprisingly, the trends and evolutions of all the variables do not indicate significant differences with change in TW conditions. It can be suggested that all the TW conditions considered in the present study are subjected to severe confinement effects. It would have been beneficial to conduct experiments at deep TW conditions. Unfortunately, the present set-up do not permit experiments at greater TW depths.

4.7 PIV and LDA assessment

This section is an assessment of the relative performances of LDA and PIV. LDA is a recognized and a well established non-intrusive technique for fluid velocity measurement while PIV though advanced, is still in its developing stages (Hyun et.al, 2003). One can obtain new insights to study coherent structures as PIV provides instantaneous global velocity fields which are not possible with pointwise techniques. LDA is largely a single point measuring technique and does not directly provide information on the spatial structure of the flow. Combining LDA and PIV techniques to investigate flows permit a more detailed interpretation of velocity fluctuations than that from LDA alone. This can be necessary when comparing measurements with numerical simulations such as LES. This section compares the mean and the turbulence intensities near the nozzle opening for a jet expanding in a tailwater of 2.5B.

Figure 4.16 shows the instantaneous velocity vectors at four different instances separated by a time of 1sec. The flow along the edges of the jet is clearly unsteady with fluid entering and leaving the jet at various locations. The region of constant velocity (potential core) appears to extend up to about X/B = 2.5. Clearly this type of spatial structure of the flow cannot be obtained by LDA. Figure 4.17 shows the average velocity field. The measurements performed with LDA is laborious. PIV measurements provide more information about velocity measurements at various sections. The profile was extracted from the average of 2000 PIV velocity fields and shows that the profiles are very close to uniform.

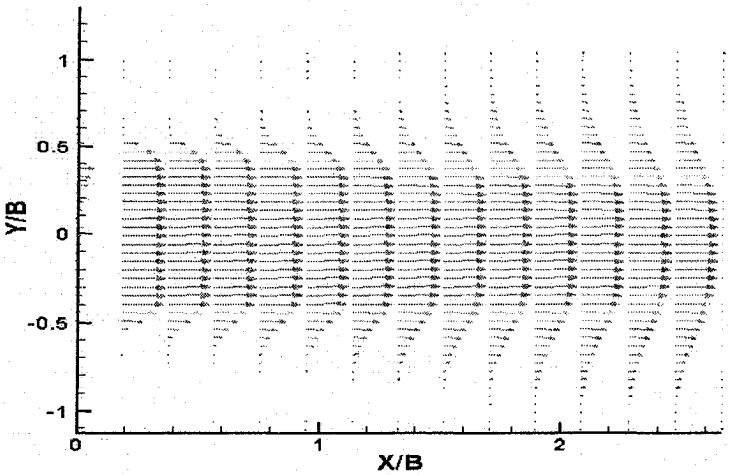

Figure 4.17: Average vector field

a) Mean velocity

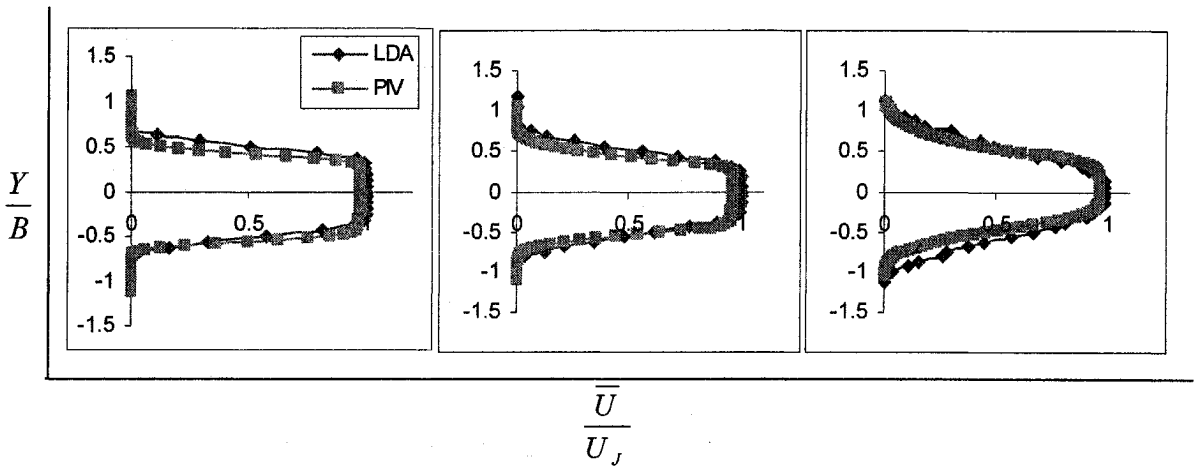

Figure 4.18: Mean velocity comparison between PIV and LDA

The PIV measurements in general confirms to the LDA measurements described earlier. However it is worthwhile to note that several of these profiles would be very laborious process with the LDA. Further, comparison of the LDA measurements with the PIV is shown in Figure 4.18. Close to the centreline ($Y/B = \pm 0.5$) the PIV and LDA data collapse onto each other. However small differences are observed at other locations. This could be possible because the measurements with LDA are statistically more

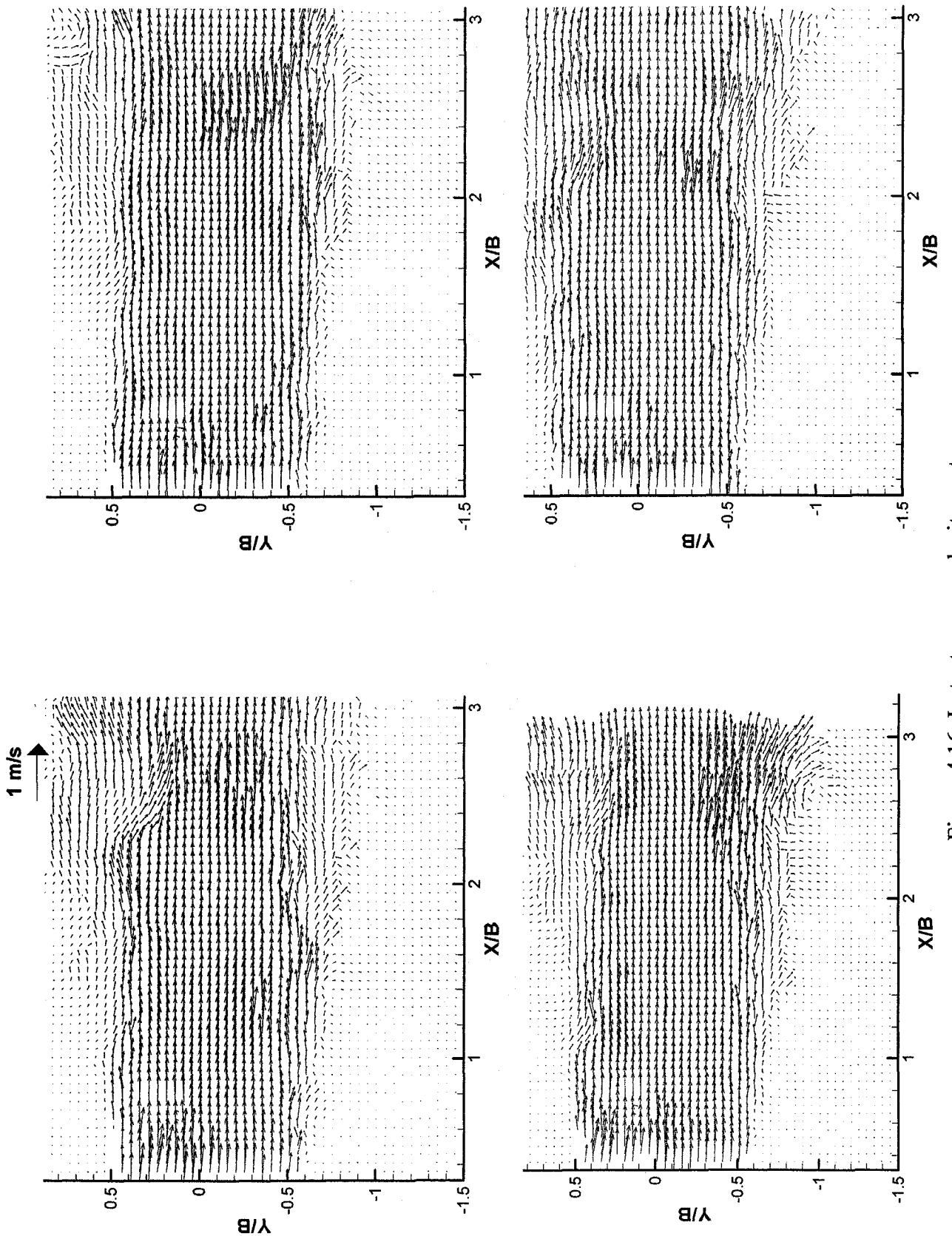

Figure 4.16: Instantaneous velocity vectors

accurate, due to the large sample size, whereas PIV measurements depend on the number of images and the frequency of acquisition.

b) Turbulence intensity

The streamwise and normal component of velocities obtained by LDA and PIV data is compared in Figure 4.21. It can be clearly seen that the high shear regions at the edges of the jet produce highest turbulence intensity. Comparatively lower values are observed in PIV data and can be attributed to the smaller number of image pairs used for the analysis. Differences are observed in the regions of high shear.

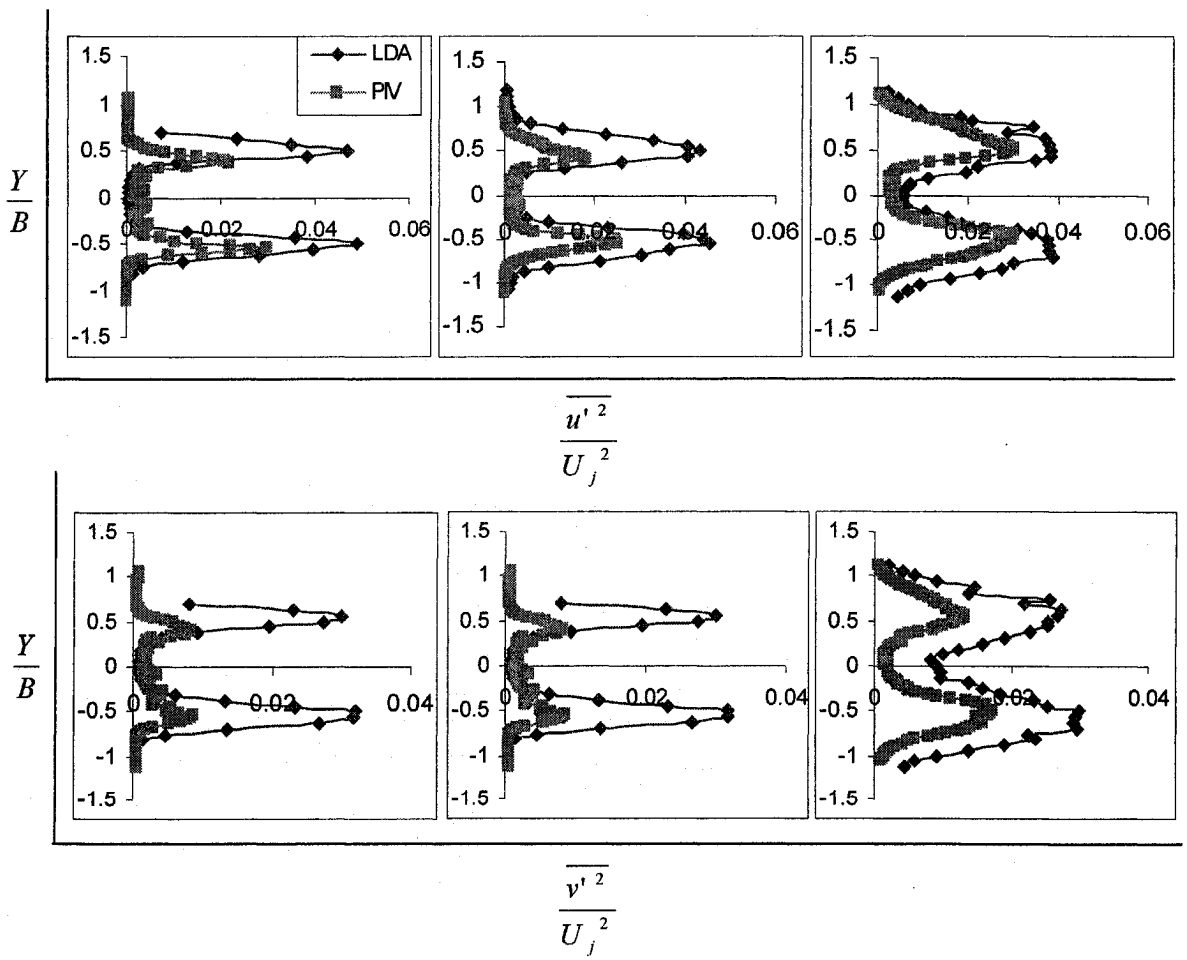

Figure 4.19: Comparison of streamwise and normal turbulence intensities of PIV and LDA

However, the overall features are still retained and can be noted from the distinct peaks at the high shear region. Good agreement is noticed at the potential core region. With increasing downstream distance the PIV values in the high local shear region are observed to be closer to the LDA values. This shows that the present PIV configuration cannot recognize particle displacement in regions of high turbulence.

As indicated earlier, the LDA measurements have a sample size of 10,000 acquired over 3 minutes. The PIV images are acquired over a time period of 10 minutes. The tendency of randomness is pronounced in the LDA data. Consequently, the PIV measurements tend to be lower than the LDA measurements. It is also noteworthy that long term PIV measurements will tend to be more random that the short term LDA measurements.

4.8 Coherent Structures

The prevalence of orderly large scale vertical structures in the near exit field of a jet has been recognized for quite sometime. There is evidence now that suggests that these vortical structures control the initial growth of turbulent jets. Most coherent structure studies have been based on flow visualization. The development of PIV provides new possibilities to further study these structures. The purpose of this section is to investigate large scale structures near the jet exit upto X/B = 3.

This section presents selected instantaneous velocity fields for a TW depth of 2.5B. An effort is made to understand the behavior of the coherent structures. A coherent structure is defined as a connected, large-scale, turbulent fluid mass with instantaneously phase-correlated vorticity over its spatial extent (Hussain, 1981). The focus is on the near- field as previous studies have shown that the exit conditions have a significant influence on the downstream evolution of the jet. Furthermore, the present LDV data analysis has indicated the presence of turbulent eddies in the near field region. The eduction of coherent structures will assist in understanding the role of vertical structures on mixing. The images presented here were taken at a framing rate of 1Hz. This time separation is too large to follow the same vortical structure in successive frames. However, an effort is made to track them. It should be noted that all the results presented in this section correspond to vortices in the x-y plane, but in actual vortices are three-dimensional.

Figure 4.16 shows the instantaneous velocity fields for 4 successive image pairs. Obviously the images do indicate randomness and unsteady flow, but do not reveal details of coherent structures. In order to identify these structures the Galilean

decomposition was performed (Adrian et. al, 2000). This involves subtracting a certain % of the jet exit velocity from the instantaneous vectors. Different proportions were attempted and 0.6 % of the instantaneous velocity was seen to reveal coherent structures (Figure 4.20). For the present frame this will be very close to the convection velocity of the vortices. Not all the vortices are exposed in such a decomposition. Vortices are observed at different locations above and below the jet centerline and some are highlighted by circles A, B etc. It is seen that with increasing distance from the nozzle the size of these structures also increase. Clockwise and counter clockwise structures are seen below and above the jet centerline respectively. It can also be noted from the Figure 4.20 that the location and size of these structures varies from frame to frame.

The rotational characteristic of eddies at the edges of the jet is responsible for directing flow into and out of the body of the jet. A recent study by Shineeb et.al, (2005) indicates the presence of vortices in pairs on either side of the jet centerline. The preliminary analysis performed in this study is not sufficient to observe this behavior. Extensive image analysis has to be carried out to identify this phenomenon.

Referring back to the quadrant analysis presented earlier, one notes that in the upper regions of the jet Q1 and Q3 dominate the flow. For the purpose of analysis, consider vortex **A** whose leading edge has just crossed the point **P** in frame 1 of Figure 4.20. As the vortex enters the point **P**, one would measure events that corresponds to Q1 and Q2 (+ ve normal component of velocity). When the trailing edge of vortex **A** is at the same point **P** one would expect events corresponding to events Q3 and Q4. We therefore would notice both Q1 and Q3 dominating the flow field above the jet centerline. These events arise due to the formation and rotation of these vortices. Such vortices can be

distinguished only with the aid of PIV measurements. This type of analysis conforms to the LDV measurements made earlier, but the coherence of the structures are more distinct. Consequently, PIV provides an enhanced view of these structures.

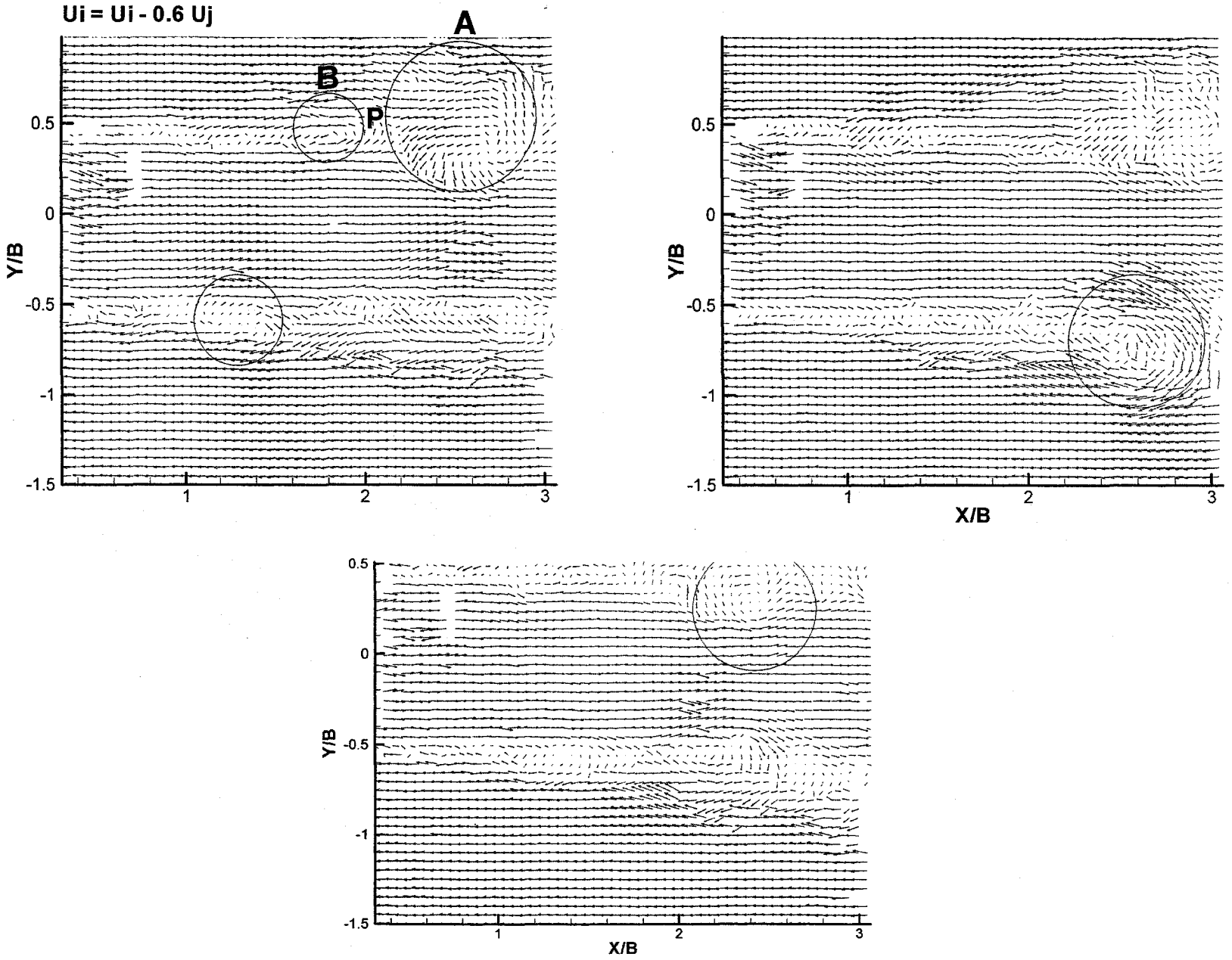

Figure 4.20: Example of coherent structures obtained using Galilean decomposition

CHAPTER 5

CONCLUSIONS AND RECOMMENDATIONS FOR FUTURE WORK

5.1 Conclusions

The present study is an experimental investigation of a turbulent square jet using LDA and PIV. The Reynolds number based on the exit condition was 40,000. The profiles were obtained both in the very-near regions ($0.5 \leq X/B \leq 3$) and in the farther regions ($3 \leq X/B \leq 27$). The mean velocity, turbulence intensity, higher-order moments and spread rate along the centreline of the jet were also obtained.

The main objective of this study was to investigate the turbulent characteristics of a square jet expanding in the vicinity of the free surface. A good comprehension of the fluid dynamics of a square jet is achieved. Quadrant analysis was performed to study the role of ejections and sweep like events. In order to track the coherent structures a Galilean transformation was performed on the PIV data. Specific conclusions are summarized below:

- The expansion of present jet is found to be greater than that of round free jets. The traditional extent of ZFE and ZEF noticed in round jets are not distinguishable for the present jets.
- At shallow tailwater conditions the jet appears to be influenced by the free surface at locations very close to the nozzle. The velocity profiles become asymmetrical following jet impingement and deformation the free surface. For the tests with deeper tailwater conditions, the mean velocity characteristics are retained for greater downstream distances from the nozzle exit compared to shallow tailwater depths.

- The present square jet is seen to completely diffuse by 27B, whereas a traditional free jet will be attaining self-similarity at this stage. No state of self-preservation is noticed in the present study.
- The deformation of the free surface and its effects on the formation of the surface waves influences the vortex formation and consequently affects the turbulence level in the jet. The measurements show that near the jet centerline, the rms fluctuations become anisotropic.
- Following jet impingement, the vertical spread is reduced. The vertical spread of the present jet is less than that of a square free jet considered by Quinn and Militzer (1992). The inhibition of the vertical spread will enhance the lateral spread.
- Under the conditions investigated, the jet profiles indicate antisymmetrical shear stress distribution. The presence of the free surface alters the shear distribution with lower values closer to the free surface. Following jet impingement, free surface effects propagate into the jet. With increasing downstream distance, the jet reaches a state where it loses jet-like characteristics at locations closer to the free surface while retaining jet properties at the bottom.
- Shear stress profiles indicate that the mixing zone formed at the bottom of the jet is significantly greater than the mixing zone on the top.
- Higher order moments indicate than there is more turbulent activity (entering and ejecting eddies) in the bottom than at the top regions of the jet. The difference in magnitudes of the peaks indicate differences in the prevailing

entrainment characteristics. Also, it is observed that the free surface suppresses the normal velocity fluctuations.

- The transverse velocity profiles indicate the presence of axis switching.
- The results were obtained with a single point technique (LDA) and a multipoint image analysis (PIV); such results are in good agreement in describing the flow configuration and the mean velocity field at different downstream locations. Differences are observed in the turbulence intensity profiles with lower PIV values observed due to the less number of images acquired.
- Galilean decomposition reveals the presence of coherent structures in the flow. The size of these structures increase with increasing downstream distances from the nozzle. Intermittent formation of these structures make the fluid dynamics in jets complicated.

The comprehensive data obtained will be helpful to validate future numerical models.

5.2 Recommendations for Future Work

The research presented in this thesis has come a long way in understanding the jet dynamics near a free surface, the following recommendations are relevant for future work:

1) Detailed analysis with PIV has to be performed to track coherent structures and investigate their effect in the flow.

2) To further investigate the behavior near the free surface.

3) To perform a CFD to analyze the free surface phenomenon and compare it with the existing data.

References

Abdel-Rahman, A. A, Chakroun, W & Al- Fahed, S. F. (1997), LDA measurements in the turbulent round jet. Mechanics research communications. Vol. 24, No.3, pp 277- 288.

Adrian, R. J, Christensen, K. T & Liu, Z. C. (2000), Analysis and interpretation of instantaneous turbulent velocity fields. *Experiments in Fluids*. Vol. 29, pp 275- 290.

Anthony, D. G, Hirsa, A & Willmarth, W. W. (1991), On the interaction of a submerged turbulent jet with a clean or contaminated free surface. *Physics of fluids* Vol. 3, No. 2, pp 245- 247.

Anthony, D. G & Willmarth, W. W. (1992), Turbulence measurements in a round jet beneath a free surface, *J. Fluid Mech*, Vol. 243, pp 699- 720.

Antonia, R. A, Xu, G (2002). Effect of different initial conditions on a turbulent round free jet. *Experiments in Fluids*, Vol 33, pp 677-683.

Cenedese, A. Doglia, G. Romano, G. P, De Michele, G, Tanzini, G.(1994). LDA and PIV measurements in free jets, *Experimental thermal and fluid science*, pp 125- 134.

Chua, L. P, Li, Y. F & Zhou, T. (2004). Measurements in a heated square jet. *AIAA Journal*, Vol. 42, No.3, pp.578-588.

Chua, L. P, Lua, A. C (1998). Measurements of a Confined jet. *Physics of Fluids*, Vol. 10, No. 3, pp 3137- 3144.

Duplessis, M. P, Wang, R. L, Kahawita, R. (1974). Investigation of the near- region of a square jet. ASME - *Fluids Engineering Division*, No. 74, FE-6, pp 246-251.

Foss, J. F. and Jones, J. B. (1968), Secondary flow in a bounded rectangular jet, Trans. of the ASME, *J. Basic Engrg.*, pp. 241-248.

Grinstein, F. F, Gutmark, E & Parr, T. (1995), Near field dynamics of subsonic free square jets. A computational and experimental study. *Physics of fluids* Vol. 7, No 6, pp 1483- 1497.

Gutmark, E and Grinstein, F. F. (1999), Flow control with non-circular jets. *Annual review of Fluid Mech.* pp 239- 272.

Hussain, A. K. M. F. & Clark, A. R. (1981), On the coherent structure of the axisymmetric mixing layer: a flow- visualization study. *J. Fluid Mechanics*, Vol. 104, pp 263-294.

Hussain, A. K. M. F & Zedan, M. F (1978 a), Effects of the initial conditions on the axisymmtric free shear layer: Effect of the initial fluctuation level. *Physics of fluids,* Vol. 21, No 9, pp 1475-1481.

Hussain, A. K. M. F & Zedan, M. F (1978 b), Effects of the initial conditions on the axisymmtric free shear layer: Effect of the initial momentum thickness. *Physics of fluids,* Vol. 21, No 7, pp 1100-1112.

Hussein, J. H, Capp, S. P, George, W. K. (1994). Velocity measurements in a high Reynolds-number, momentum-conserving, axi-symmetric, turbulent jet. *Journal of Fluid Mechanics*, Vol. 258, pp 31- 75.

Liepman, D. & Gharib, M. (1994). The Vorticity and Entrainment Dynamics of near - surface jets. *Trans ASME*, FED-181, pp 53-58.

Lu, S. S & Willmarth, W. W. (1973). Measurements of the structure of the Reynolds stress in a turbulent boundary layer. *Journal of Fluid Mechanics,* Vol. 60, pp 481–511.

Miller, R. S, Madina, C. K & Givi, P. (1995). Numerical simulation of non- circular jets, *Computers and Fluids,* Vol. 24, No. 1, pp 1-25.

Morel, T (1975). Comprehensive design of asi-symmteric wind tunnel contractions. A.S.M.E. Transactions, *Journal of Fluids Engineering*, Vol. 87, No. 2, pp 225-233.

Nezu, I (2005). Open-Channel Flow Turbulence and Its Research Prospect in the 21st Century. *Journal of Hydraulic Engineering*, Vol. 131, No. 4, pp. 229-246.

Quinn, W. R & Militzer, J (1988). Experimental and numerical study of turbulent free square jet. *Physics of fluids,* Vol. 31, No 5, pp 1017- 1025.

Quinn, W. R (1992), Streamwise evolution of a square jet cross section. *AIAA Journal,* Vol. 30, No. 12, pp 2852- 2857.

Rajaratnam, N. (1976), Turbulent Jets, Elsevier Scientific Publishing Company, Amsterdam.

Rajaratnam, N & Pani, B. S. (1974). Three- dimensional turbulent wall jets. *Journal of the hydraulic division* HY1 pp 69-83.

Rajaratnam, N .,& Humphries, J.A. (1984). Turbulent Non-Buoyant Surface Jets. *Journal of Hydraulic Research*, Vol. 22, No.2, pp.103- 115.

Sforza, P. M, Steiger, M. H & Trentacoste, N. (1966), Studies on three-dimensional viscous jets. *AIAA Journal,* Vol.4, No. 5, pp 800- 806.

Sforza, P. M & Trentacoste, N. (1967). Further experimental results for three-dimensional free jets, *AIAA Journal,* Vol 5, No.5, pp 885- 890.

Shineeb, A. M, Balachandar, R & Bugg, J. D. (2002), PIV measurements in a confined jet. ASME- *Fluids Engineering Division Summer Meeting*, 257(2A) pp 87- 93.

Shineeb, A. M, Balachandar, R & Bugg, J. D. (2004), PIV measurements in shallow water jets. CSCE - *Water and Environment Specialty Conference*, 211 pp 1-10.

Wygnanski, I., & Fielder, H. (1969). Some measurements in the Self- Preserving Jet. *Journal of Fluid Mechanics*, Vol. 38, pp. 577-612.

Appendix A

Uncertainty Analysis

This section contains the error estimation for the results reported in this study. The uncertainties in the mean measurements are quantified. The main source of error in the LDA measurements is the uncertainty in the determination of the frequency present in each burst of the processor. In addition to the above, the uncertainty in statistical quantities will also depend on the sample size (N).

A methodology for estimating uncertainty in LDA measurements was developed by Yanta and Smith (1973) and Schwarz et al. (1999). They derived the following relations for the uncertainty in the streamwise and vertical components of the mean velocity respectively:

$$\frac{\sigma_U}{\overline{U}} = \left[(\sigma_o)^2 + \frac{1}{N}\left(\frac{u}{U}\right)^2 \right]^{1/2} \qquad \text{Eq.1}$$

$$\frac{\sigma_V}{\overline{V}} = \left[(\sigma_o)^2 + \frac{1}{N}\left(\frac{v}{V}\right)^2 \right]^{1/2} \qquad \text{Eq. 2}$$

where σ_o is the error due to the uncertainty in the determination of the beam-crossing angle and N is the number of samples.

The corresponding expressions for the streamwise and vertical components of the turbulence fluctuations and the Reynolds shear stress are respectively given by:

$$\frac{\sigma_u}{u} = \left[(\sigma_o)^2 \left(\frac{\langle uv \rangle}{u^2} \right) + \frac{1}{2N} \right]^{1/2} \qquad \text{Eq. 3}$$

$$\frac{\sigma_v}{v} = \left[(\sigma_o)^2 \left(\frac{\langle uv \rangle}{v^2} \right) + \frac{1}{2N} \right]^{1/2} \qquad \text{Eq. 4}$$

$$\frac{\sigma_{\langle uv \rangle}}{\langle uv \rangle} = \left[(\sigma_o)^2 \left(1 + \frac{u^2}{\langle uv \rangle} \right)^2 + \frac{1}{N} \left(\frac{2}{R} \right) \right]^{1/2} \qquad \text{Eq. 5}$$

R is the shear stress correlation coefficient.

Following Schwarz et al. (1999) a value of $\sigma_o = 0.4$ is adopted in the present analysis. Typical estimates of uncertainties for the mean and fluctuating quantities are given in Table A using the test conditions for a Tailwater depth of 2.5B.

$\bar{U}$ (%)	u (%)	v (%)	$\langle uv \rangle$ (%)
4.0	6.0	5.0	7.5

Table A: Typical uncertainty estimates

It should be noted that the uncertainty estimates summarized in Table A do not consider errors due to electronic noise.

Appendix B

Data obtained from tests

The data for all the figures plotted in this thesis can be found on the enclosed CD-ROM

VITA AUCTORIS

Girish sankar was born in 1981 in Chennai, INDIA. He graduated from the Regional Engineering College, Kurukshetra, Haryana, INDIA in 2002 with a Bachelor of Technology in Civil Engineering. He was accepted in the Faculty of Graduate Studies and Research at the University of Windsor in 2003 leading to the degree of Master of Applied Science in Civil Engineering.